Digital Elevation Model Extraction from ASTER In Support of the "Coal Fire and Environmental Research Project, China"

Xiong Ping
February, 2003

Digital Elevation Model Extraction from ASTER
In Support of the
"Coal Fire and Environmental Research Project, China"

by

Xiong Ping

Thesis submitted to the International Institute for Geo-information Science and Earth Observation in partial fulfilment of the requirements for the degree of Master of Science in Geo-information Science and Earth Observation (ITC), Earth Resources and Environment Geo-sciences (EREG), Natural Hazard Studies specialisation (NHS)

Degree Assessment Board

Prof.Dr. F.D. van der meer (Chairman) ESA Department, ITC
Dr. A.C. Seijmonsbergen (External Examiner) UvA
Dr. B.H.P. Maathuis, (First Supervisor) WRS Department, ITC
Dr. P.M. van Dijk, (Second Supervisor) ESA Department, ITC

INTERNATIONAL INSTITUTE FOR GEO-INFORMATION SCIENCE AND EARTH OBSERVATION
ENSCHEDE, THE NETHERLANDS

Disclaimer

This document describes work undertaken as part of a programme of study at the International Institute for Geo-information Science and Earth Observation. All views and opinions expressed therein remain the sole responsibility of the author, and do not necessarily represent those of the institute.

Abstract

This thesis studies in DEM extraction using ASTER Band 3 nadir-backward looking image pair, within a software environment of Erdas Imagine OrthoBase pro and ArcView GIS. Suitable data application and proper operation allow for the study results acceptable. The results are close to the precision range of the ground data source.

Deriving 3D terrain information from digital stereo data is serving for multidisplinary sciences today. Other than constant field-survey, digital photogrammetric tools allow for the accurate data collection from imagery. High-resolution satellite images are lending themselves to many detailed site specific studies. Among them, ASTER (Advanced Spaceborne Thermal Emission and Reflection Radiometer) is providing data at a relatively low cost.

The coal fire and environmental research project (China) needs an economical and efficient Digital Elevation Model of the study area to support the thermal and coal fire spreading research as topographic references.

As many studies using remote sensing data to extract DEM, the data source in this case is not ideal. An ASTER L1A 3N-3B image pair covering the study area is the main data source, with some part of low-correction and clouds; a dated topographic map of 1:100,000 scale was served as the ground data; no accurate extra data were offered.

By following the basic principle of keeping GCPs evenly-distributed, adequate and accurate in all terrain types within the borders of the image pair used to extract the DEM, careful experiments and proper operations were contributed to obtaining an acceptable accuracy result of the derived DEM.

After DEM extraction, the slope and aspect elements were derived to perform day-time thermal image correction for coal fire research project.

The methodology adopted in this research is verified efficiently. For further study, higher accurate data sources and more detailed editing can improve the DEM accuracy significantly.

Acknowledgment

Table of Contents

List of Figures

List of Tables

List of Appendices

1. Introduction

1.1   Research Project

Coal fires have become a geohazard in many countries in the world these years. India, USA, Europe and Russia, South Africa, Australia, China and some other regions are affected by this environmental hazard (Figure 1.1).

Fig 1.1: Coal Fire Extension In the World   COPYRIGHT© DLR, 2002

As the largest producer of coal in the world, the People's Republic of China treats coal as the most important mineral resource for the national economy. However, uncontrolled burning of coal layers, which originates at the interface of the coal seams and the atmosphere, has caused tremendous economic and environmental problems. Up to the year 1994, the yearly losses due to coal fire, by natural and man-made reasons, were estimated at 100-200 million tons. Moreover, pollutant gases are produced from the burning. According to the statistics in 1994, the composition of the atmosphere is influenced, 2-3% of the total CO_2 emission is due to these coal fires (Rozema et al., 1993).

These fires occur within a region that stretches over 5000 km east-west and 750 km north-south in China (Figure 1.2).
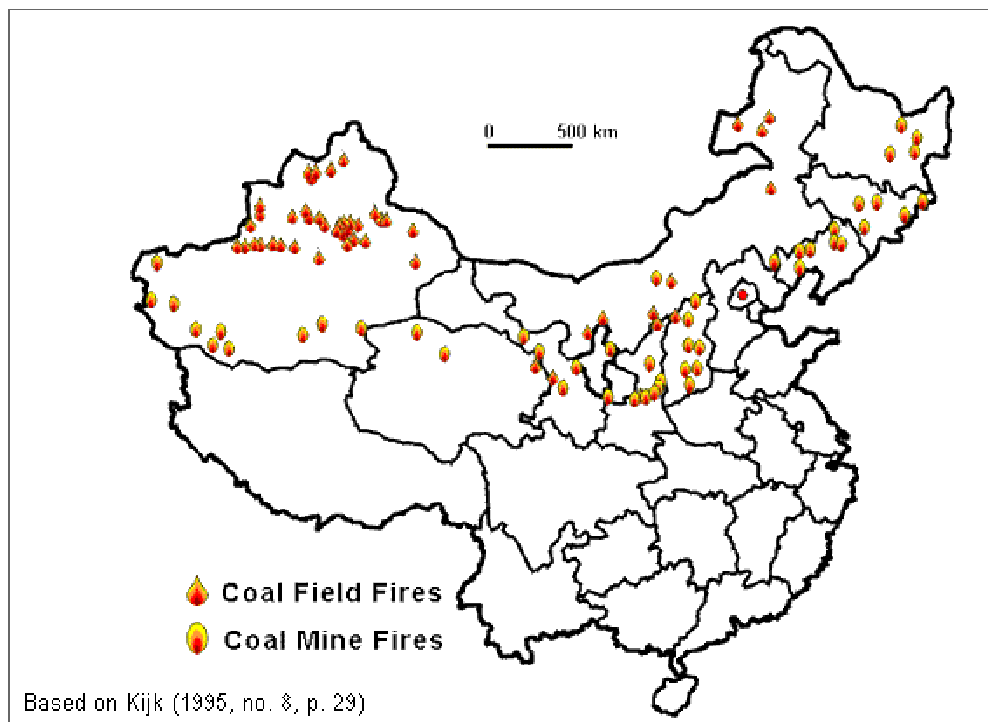
Fig 1.2: Coal Fire Distribution Map of China

In 1993, October, the "Coal Fire and Environmental Research Project, China" was identified as a mission. Three years later, in June, the contract for the development of a coal fire monitoring system was signed.

The project devotes itself to developing and implementing a system to detect, measure and locate, monitor and prevent coal fires. The ultimate objective of the coal fire project is to set up a coal fire-related information system in which thermal imagery, topographic and subsurface data are incorporated.

1.2   Motivation

In 1997, a DEM covering Kelaza area of Xinjiang Autonomous Region of China was derived from air photos by ITC and the Ministry of Coal Industry of China, and was funded by the European Commission (Figure 1.3).

With the satellite data of ERS (European Remote-Sensing Satellites, ERS-1 and ERS-2), digital elevation models with a resolution of 25m covering Ningxia and Xinjiang coalfire test areas for the project have been generated by the TU Dresden, TU Munich and Universitiy of Hohenheim (Figure 1.4). Later the test area was shifted to the northern Helan mountains for the research project. Wuda coal field needs a digital elevation model for coal fire related research.

Moreover, the DEM extracted for Wuda test area would be derived from ASTER, which is relatively cheap having a high spatial resolution, thus becoming an economical and effective way to generate a DEM.

This study will be an extension of the previous DEM achievement, to support the thermal and coal fire spreading research as topographic references in the framework of the coal fire research project.
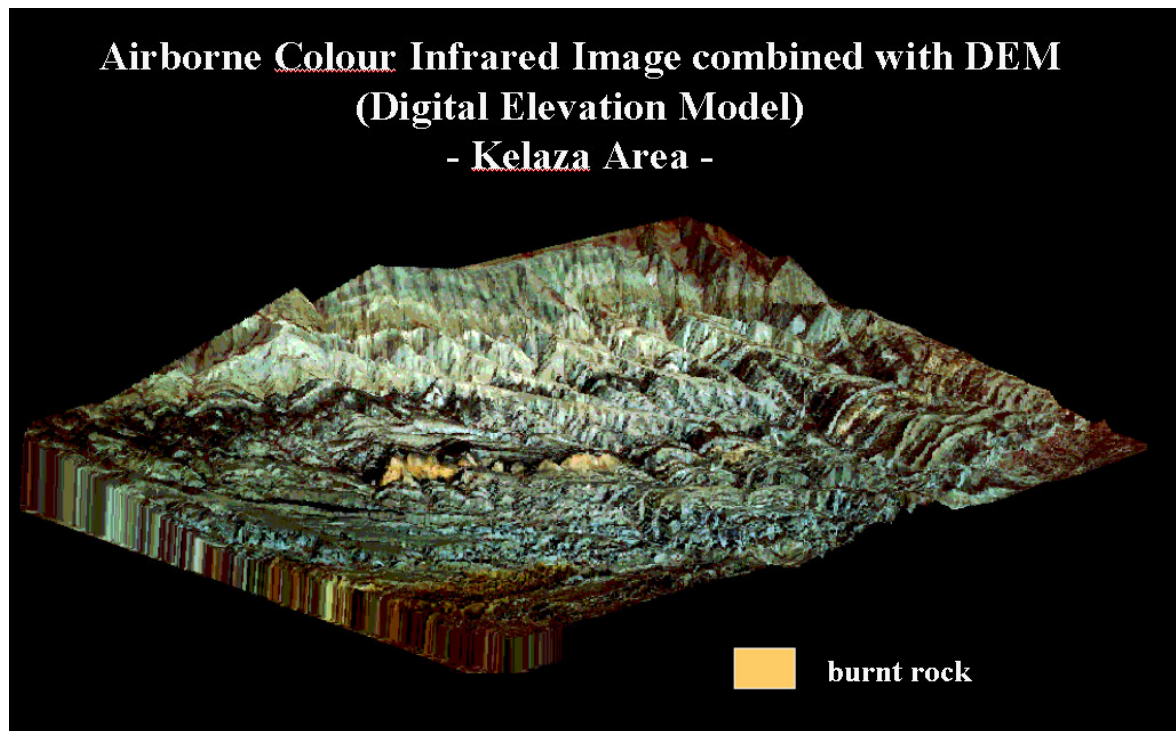
Fig 1.3: DEM extracted from air photos for Kelaza coal fire area, Xinjiang province
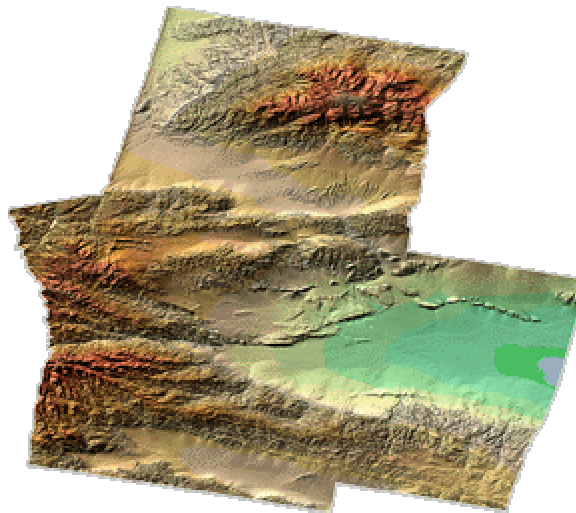
Fig 1.4: DEM Extracted from ERS for Xinjiang and Ninxia Test Areas
(provided by http://www.dfd.dlr.de/projects/coalfire/Remote_sensing_project/html/dem.html)

1.3   Research Questions

For this research, there are some questions to be solved passing through the method routine:

- How to ensure and control the accuracy of the DEM extracted from ASTER?
- What is the requirement for applying different spatial-resolution data in different area such as mountains and plain?
- How to verify and modify DEM integrating with available topographic data and spot heights?
- Which method can be used to assess the accuracy of the DEM? How to assess the accuracy for different terrain types?

1.4   Research Objectives

The research should reach the objectives as follows:

- Extraction of a DEM from ASTER Band 3N and 3B on the basis of stereo correlation-image matching techniques;
- Use of different interpolation techniques (TIN based-linear, Grid based-Inverse Distance Weighted, spline);
- DEM modification integration with existing contour line data and spot heights, including sink removal;
- Accuracy assessment of the DEM obtained (absolute X, Y, Z in different terrain types);
- Create derived products (like ortho-image, slope angle and aspect maps) needed as   input for atmospheric correction of thermal images.

1.5   Methods

This research will be achieved through the workflow as shown below (Figure 1.5):
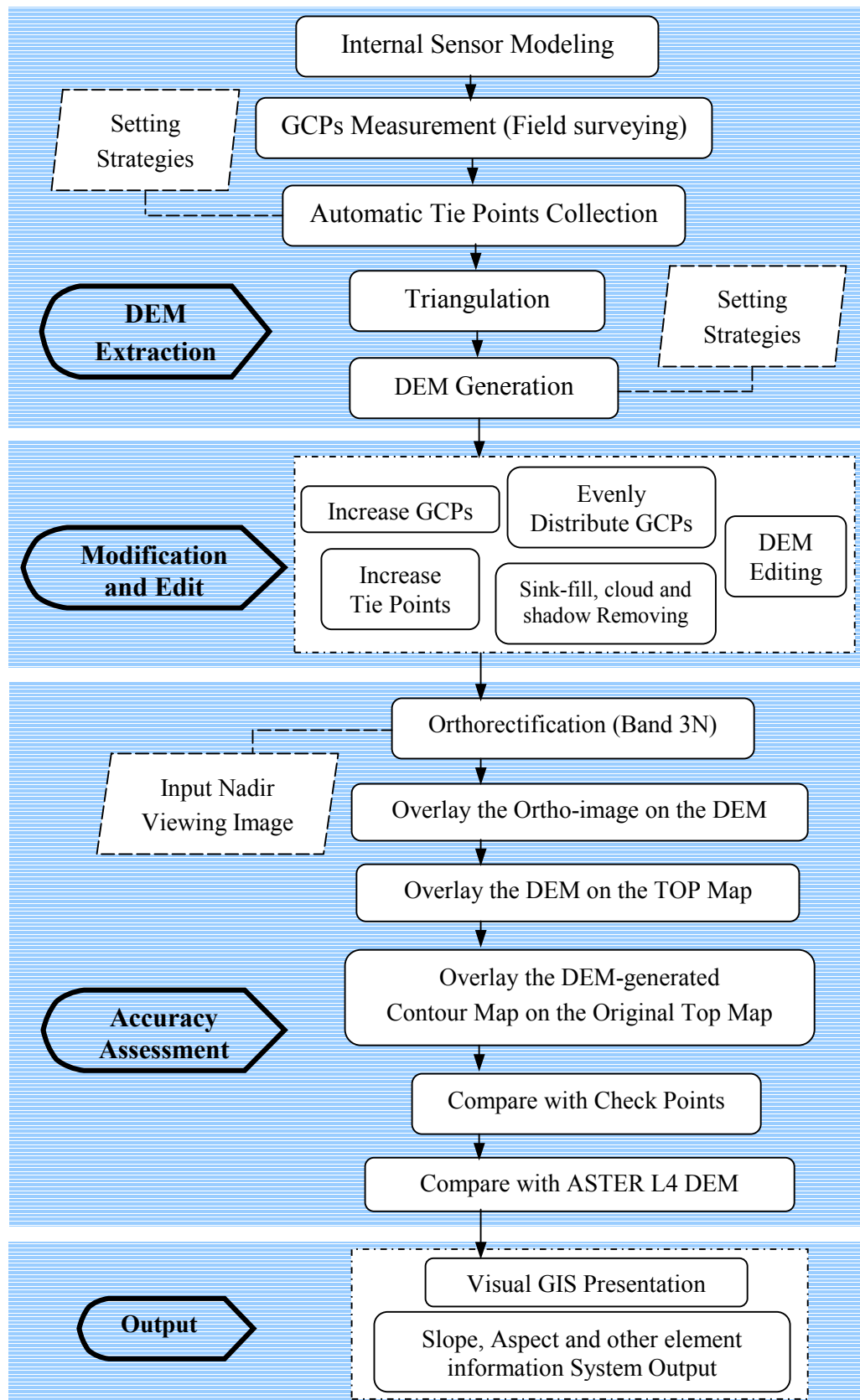
Fig 1.5: Work Flow of the Methodology

1.6   Study Area

The study area selected is situated in the nothern Helan mountains region, ranging up to 3000m between the Gobi desert and the Yellow River in northern China. They are close to the provinces Ningxia and Inner Mongolia. The coalfields include Gulaben, Ruquigou and Wuda (Figure 1.6).

Fig 1.6: Study Area Location

The test area for this study is surrounding the Wuda coal fire area. Wuda coal fire area is situated in the southwest part of Inner Mongolia Autonomous Region of China. It is close to Ningxia province, northeast of the Helan Mountain Ranges and west of the Yellow River. Wuda coal field is approximately 10 km long (N-S) and 3-4 km wide (E-W). The area covers about 35 km^2 and its relief differs between 1100 m and 1300 m above sea level (Figure 1.7).

Fig1. 7: The Terrain Relief in Wuda Coal Fire Region

The climate features are semi-arid, cold long winters with frequent blizzards, and warm short summers, belonging to continental climate type. The temperature's record low is -50°C. It is windy in all seasons, especially in spring (http://drlee.org/mongolia/innermon.html).

Agriculture is the economic mainstay here. Furthermore, small and medium-sized steel works and nonferrous metallurgical works has been developed as modern industry in this region. Multicultural people lived in this region for generations.

Wuda coalfield has become the largest coalfield fire zone in the past several decades in China. According to the investigation of China relevant government, the coal fire area increased 50% within the last 10 years, while the annual burning coal has reached 300,000 tons. Every year the fire zone emitted 5,000 tons of SO_2 into the air. Research contributed on this area has obvious significance for the coal fire project (http://www.enviroinfo.org.cn/Disasters/Fire/e012142_en.htm).

1.7   Scope of the Research

This research is focusing on the DEM extraction using ASTER Nadir-backward looking Band 3 data, on the basis of automated digital stereo-correlation image matching techniques.

Due to the limitation of the quality of the data sources, the results could be affected:

1) As for the ASTER image pair used, there are some parts on the image with low-correlation, and with some clouds, which will be an obstacle in the stereoimage matching process to generate corresponding points and interpolate mass points from the image pair.

2) The topographic map, the main ground data provider, is on a relatively smaller scale of 1:100,000, the precision request for DEM extraction is initially reduced.

3) The ground-truthing data obtained from the related fieldwork and topographic map only cover a relatively small part compared with the ASTER image range (Figure 1.8). Extra data was needed. However, due to the different error systems, this integration between field data and extra data can result in a less accurate output.
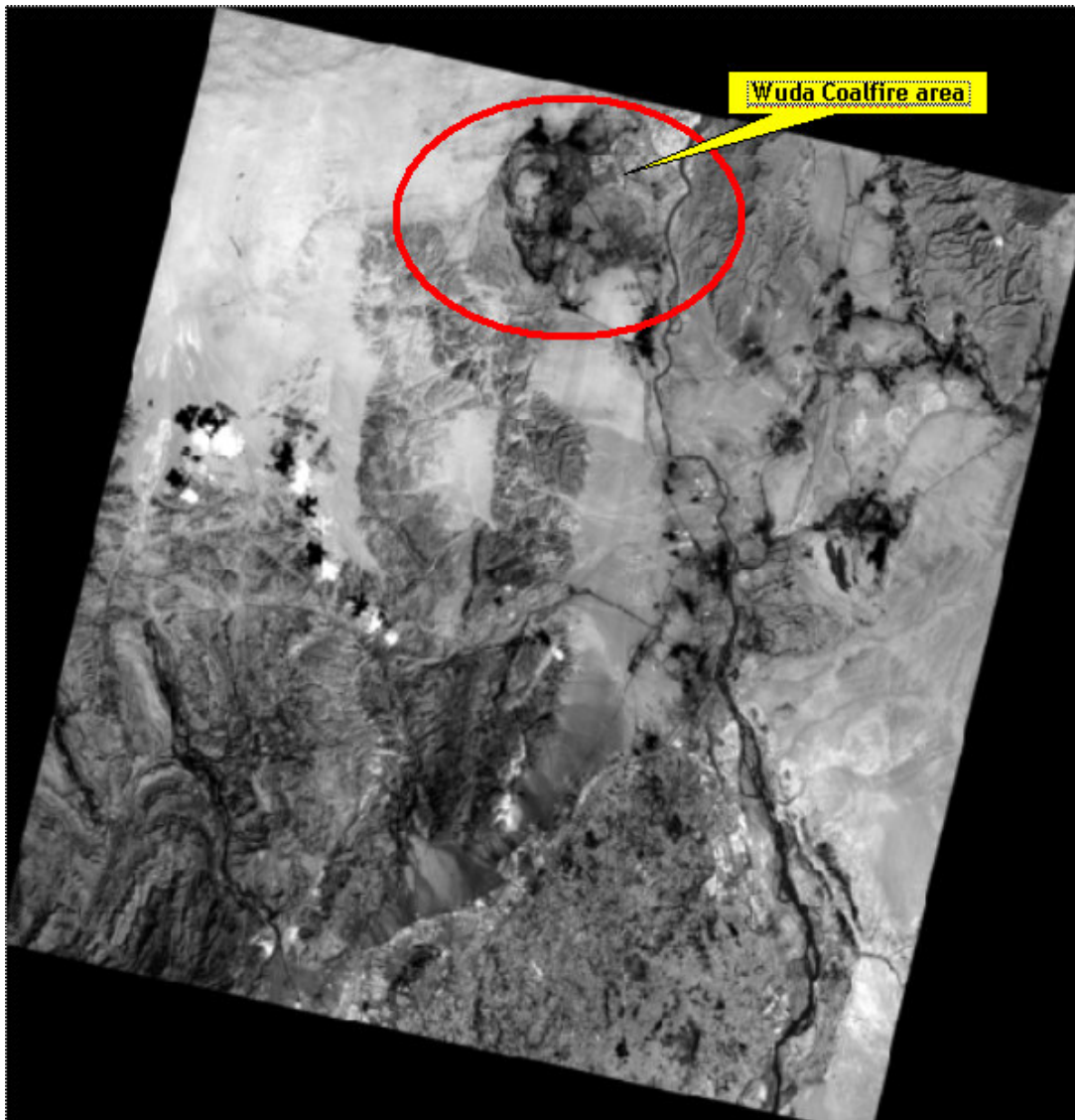
Fig 1.8: The Wuda Coal fire Area on the ASTER Image

1.8   Content of the Report

Chapter 1: Introduction. Introduce the general situation of this research, give an overview about the thesis topic.

Chapter 2: Satellite Remote Sensing for DEM Generation. Review the background knowledge related to this research.

Chapter 3: Methodology. Analyze the methods used for DEM extraction from ASTER stereo image pair in this study.

Chapter 4: DEM Extraction from ASTER Image Pair. State the experiments routine of DEM extraction, concentrating on specific complexity and difficulties met in the operation.

Chapter 5: Accuracy Assessment and Discussion. Evaluate the final results of the DEM extracted through the methodology researched in this study, with related discussions to analyze the results of accuracy assessment, presenting particular interpretation for this research topic.

Chapter 6: Output and Derived Products. Output the achievements made by this research, and derive the associated products.

Chapter 7: Conclusion and Recommendation. Make a conclusion for the research, and refer to recommendations for further study on the basis of present study.

2. Satellite Remote Sensing for DEM Generation

2.1 DEM Introduction

Photogrammetry produces accurate and precise geographic information from a wide range of photographs and images. Any measurement taken on a photogrammetrically processed photograph or image reflects a measurement taken on the ground. Rather than constantly go to the field to measure distances, areas, angles, and point positions on the Earth's surface, photogrammetric tools allow for the accurate collection of information from imagery. Photogrammetric approaches for collecting geographic information save time and money, and maintain the highest accuracy (Erdas, 2001).

Modern photogrammetry has entered a digital era. The advanced technology of data collection, processing, storage and production is serving for multidisciplinary fields. Land surface study has been developed by utilizing digital topographic data, which is characterized by elevation of points (spot height) and contour lines. Today, the relative surface products such as digital elevation model (DEM), triangular irregular networks (TIN), or digital terrain model (DTM) can be derived even without ground-truth data, for example, utilizing ephemeris data that include sensor geometry information when an image was captured. Afterwards, contour maps, slope maps and other related information can be obtained on the basis of above-mentioned products. These topographic data is used to study the nature of the terrain to aid decision making.

2.1.1 Definition

Jaurequi (1984) defines a digital elevation model (DEM) as a statistical representation of continuous surface of the ground by a large number of selected points with known x,y,z co-ordinate fields. Aronoff (1990) argues that they are a set of elevation measurements for locations distributed over the land surface and that it carries different names; *digital elevation model, digital terrain model, digital terrain data.* Meijerink et al (1994), differentiates a DEM from a DTM. He defines a digital terrain model as a spatial distribution of terrain attributes, a topographic map in digital format, that not only consists of the DEM but also slope, aspect, the types of land use, settlements, types of drainage lines and so on. In general, a digital elevation model (DEM) is a digital file consisting of terrain elevations, and a DTM consists of additional terrain information.

2.1.2 Application

DEM is important for land surface processes, hydrologic and hydraulic modeling, assessment of land resources, management of watersheds and ecosystems, calculation of rock volumes. They are particularly useful for (http://www.spotimage.fr/home/proser/elevat/dem/welcome.html):

- Site selection and monitoring
- Impact studies
- Mobile telecommunication network engineering
- Structural geological studies

- Mission planning
- Defence simulation
- Geographic Information Systems

DEMs form the basis of many GIS applications including watershed analysis, line of sight (LOS) analysis, road and highway design, and geological bedform discrimination. DEMs are also vital for the creation of orthorectified images (Erdas, 2001).

2.1.3 Types

A DEM can appear in different formats. Normally the choice can be made from: point model, line model, grid/raster model, or the triangular irregular network (TIN) (Kiyingi, 1998).

- Point Model.

  In this model, elevations are described by a certain amount of points. For a particular point, z coordinates are added to corresponding x, y coordinates. Spatial analysis like interpolation can be applied to the point data.

- Line Model.

  The terrain is described by contours whose elevations (z coordinates) are kept constant for the x, y coordinates along the contour. Interpolation can be made to derive the elevations of points in between adjacent contours. Simple overlay analysis can be done on thematic maps (Ramroop 1995) or remotely sensed data in order to determine the elevation and hence the delineation of zones for decision making.

- Raster/grid Structure

  DEMs in raster format display in gray scale where bright areas represent high elevations, dark areas represent low elevations.

  This is one of the most common forms of DEMs. This kind of DEMs describe the terrain by a sampled array of elevations for a number of ground positions at regularly spaced intervals (Moore et al. 1991). Computer implementation applied to rectangular arrays of elevations tends to be more effective. A disadvantage associated with DEMs in this format is that for large areas of level or uniformly sloping terrain, a great deal of computer memory is wasted storing highly redundant elevation information. More complex data structures such as *quadtrees* can be used in lieu of arrays to reduce storage requirements of regular grids; however, their implementation is far more complicated. Normally, this kind of problems can be overcome by data compression, and depend on the precision of z values.

  This model is simple and tends to be more efficient than other models. Elevation data in grid format is relatively abundant and inexpensive. But some time when the terrain is with much variability, or there are linear features used for large-scale application, this format could lose information between pixels.

- Triangular Irregular Network (TIN).

  This model is the other of the most common forms of DEMs, based on point, line and triangle structure. A TIN is a set of nonoverlapping contiguous triangular facets of irregular sizes and shapes. The Delaunay triangulation approach is used to create a TIN from mass points. In a Delaunay triangulation, the lines are drawn between points in closest proximity to each other, without any lines intersecting. The resulting set of triangles has the property that for each

triangle, the circle that passes through the three vertices contains no vertices of any other triangles. The vertices that make up these areas are triangulated points, but are not necessarily present at regular postings. The edges of triangles are formed by lines joining the points with x, y, z coordinates, without any intersection. Each triangle side has a uniform slope. A TIN affords a more efficient representation of terrain in terms of data storage. Elements of terrain (slope and aspects) can better be visualized in this model.

This model can consider the variability of the terrain, and is able to represent linear features precisely by enforcing them as edges of corresponding triangular facets. However, the data processing and building tend to be less efficient than grid model. (Esri, 2002)

Grids are usually used more for regional, small-scale applications, while TINs are used for more detailed, larger scale applications. Use a grid if your source data's positional accuracy isn't very high or you don't need to represent linear features like roads and streams exactly. On the other hand, if your source data is very accurate and you would like it maintained, or you need to represent linear features, use a TIN (Esri, 2002).

2.1.4 DEM Generation

There are a number of production strategies to collect digital elevation data in modern scientific technologies, including manual profiling from photogrammetric stereomodels, stereomodel digitizing of contours, digitizing topographic contour maps, converting hypsographic and hydrographic tagged vector files, and performing autocorrelation via automated photogrammetric systems. Of these techniques, the derivation of DEM's from vector hypsographic data produces one of the most accurate model. Moreover, due to the difficulty of collecting relevant data and the expensive production procedure, using satellite data to produce DEM has been a recent development research topic. DEM can be generated by automatically correlating Remote Sensing images.

In general, several phases have to be passed through to create and then use a DEM. The performance of DEM processes (Tempfli 1994) must be oriented towards achieving the following:

- Accuracy (precision and comprehension),
- Appearance (of the derived products),
- Efficiency (with respect to time and cost),
- Reliability (in operations if made use of),
- Simplicity (of operations) and
- Versatility (of the DEM system to the users).

The main operations to achieve the above, are shown in the diagram below (after Tempfli, 1994):
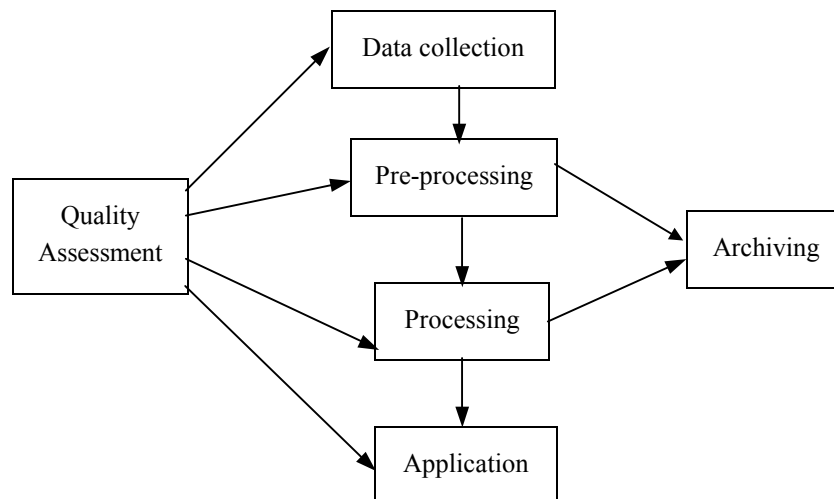
Fig 2.1: The relationship between the main operations for DEM generation

2.1.4.1 Interior Orientation and Exterior Orientation

Many photogrammetric tasks can be highly automated in digital photogrammetry (e.g., automatic DEM extraction and digital orthophoto generation). Digital photogrammetry is photogrammetry as applied to digital images that are stored and processed on a computer. Digital images can be scanned from photographs or can be directly captured by satellite sensors.

For any of the aforementioned photogrammetric tasks to be undertaken, a relationship between the sensor, the image(s) in a project, and the ground must be defined. The following variables are used to define the relationship:

• exterior orientation parameters for each image
• interior orientation parameters for each image
• accurate representation of the ground

In order to process the various types of photography and imagery, the appropriate sensor model that defines the geometry of the sensor must be selected. The geometric properties of a sensor model define the internal and external characteristics associated with a sensor model. Each sensor type has different internal and external properties associated with it. This information is required for point determination and the creation of orthorectified images, DEMs, and stereopairs (Erdas, 2001).

Internal characteristics include parameters that define the internal geometry of the sensors as they existed when the imagery was captured. The variables associated with image space are defined during the process of defining interior orientation. Interior orientation is primarily used to transform the image pixel coordinate system or other image coordinate measurement system to the image space coordinate system.

External parameters define the original position and orientation of the sensor when the imagery was captured, by using the X, Y, and Z coordinates of the exposure station and the rotational elements as the degree of tilt in each image expressed by omega, phi and kappa.

The optimal situation is to import these parameters directly from one of the following sources:

- Airborne GPS (Global Positioning System) and INS (Inertial Navigation System) data.
- Existing photogrammetric workstations.
- Initial values approximated from topographic maps.

The availability of the exterior orientation parameters advances the automation of the whole procedure of creating orthorectified images. With highly accurate exterior orientation values, the automatic workflow can be shortened, even not requiring manual measurement of GCPs and triangulation (ERDAS, 2001). Additionally, the values of exterior orientation on a given level of accuracy can ensure a high accuracy on the exterior orientation parameters approximation and the absolute x, y, z coordinates measurements.

As Figure 2.2 shows, the original position and orientation of the sensor can be defined by Xo, Yo, Zo and Omega (ω), Phi (φ), Kappa (κ). They define the position of the perspective center (O) with respect to the ground space coordinate system (X, *Y,* and Z); and the angular elements: Omega is a rotation about the photographic x-axis, Phi is a rotation about the photographic y-axis, and Kappa is a rotation about the photographic z-axis.
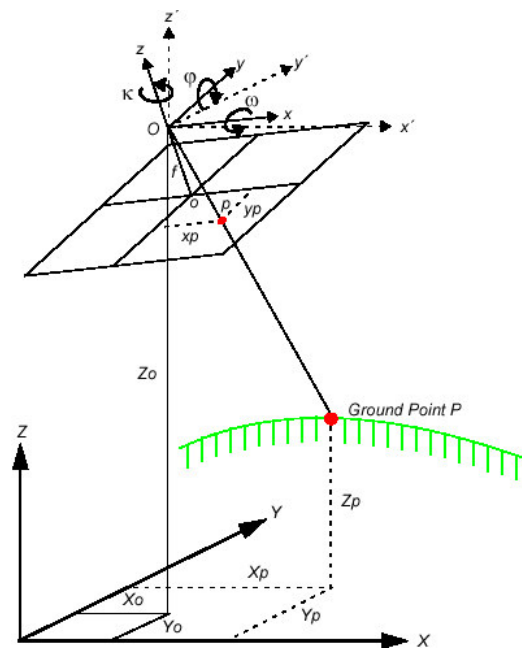
Fig 2.2: Elements of exterior orientation

Collinearity Condition The relationship between the sensor, the image, and the ground commonly uses the collinearity condition. The collinearity condition specifies that the exposure station, ground point, and its corresponding image point location must all lie along a straight line, thereby being collinear. Two equations comprise the collinearity condition:

$$x_p - x_o = -f\left[\frac{m_{11}(X_p - X_{O_1}) + m_{12}(Y_p - Y_{O_1}) + m_{13}(Z_p - Z_{O_1})}{m_{31}(X_p - X_{O_1}) + m_{32}(Y_p - Y_{O_1}) + m_{33}(Z_p - Z_{O_1})}\right]$$

$$y_p - y_o = -f\left[\frac{m_{21}(X_p - X_{O_1}) + m_{22}(Y_p - Y_{O_1}) + m_{23}(Z_p - Z_{O_1})}{m_{31}(X_p - X_{O_1}) + m_{32}(Y_p - Y_{O_1}) + m_{33}(Z_p - Z_{O_1})}\right]$$

Where:

$$M_{11} = \cos\varphi \times \cos\kappa$$
$$M_{12} = -\cos\varphi \times \sin\kappa$$
$$M_{13} = \sin\varphi$$

$$M_{21} = \cos\omega \times \sin\kappa + \sin\omega \times \sin\varphi \times \cos\kappa$$
$$M_{22} = \cos\omega \times \cos\kappa - \sin\omega \times \sin\varphi \times \sin\kappa$$
$$M_{23} = \sin\omega \times \cos\varphi$$

$$M_{31} = \sin\omega \times \sin\kappa - \cos\omega \times \sin\varphi \times \cos\kappa$$
$$M_{32} = \sin\omega \times \cos\kappa + \cos\omega \times \sin\varphi \times \sin\kappa$$
$$M_{33} = \cos\omega \times \cos\varphi$$

Once each observation equation is formulated, the collinearity condition can be solved using an approach referred to as least squares adjustment.
The photogrammetric modeling based on collinearity equations eliminates distortion errors most efficiently, and creates the most reliable orthoimages.

Least squares adjustment is a statistical technique that is used to:
• estimate or adjust the values associated with exterior orientation
• estimate the X, Y, and Z coordinates associated with tie points
• estimate or adjust the values associated with interior orientation
• minimize and distribute data error through the network of observations

The least squares approach requires iterative processing until a solution (for example space forward intersection technique) is attained. A solution is obtained when the residuals, or errors, associated with the input data are minimized.

2.1.4.2 Image Matching Geometric Constraint

For ensuring highly accurate and reliable image matching effect, the geometric and radiometric characteristics (derived from sensor model information and image gray values) associated with the stereopairs are used to performance the image matching constraint (Erdas, 2001).
Conceptually, a stereopair includes two images that come from rays projected from the terrain, through the sensors, onto an image plane that has a particular position and attitude (Lillesand, 2000).
The most common constraint is epipolar geometry. Epipolar geometry is also commonly associated

with the coplanarity condition. The coplanarity condition states that the two sensor exposure stations of a stereopair, any ground point, and the corresponding image position on the two images must all lie in a common plane. The common plane is also referred to as the epipolar plane. The epipolar plane intersects the left and right images, and the lines of intersection are referred to as epipolar lines. The image positions of a ground point appearing on the left and right photos lie along the epipolar line. Figure 2.3 illustrates the image matching process using epipolar geometry as a geometric constraint. Where P is the ground point. Xp, Yp and Zp mark the location of the image point in ground space.
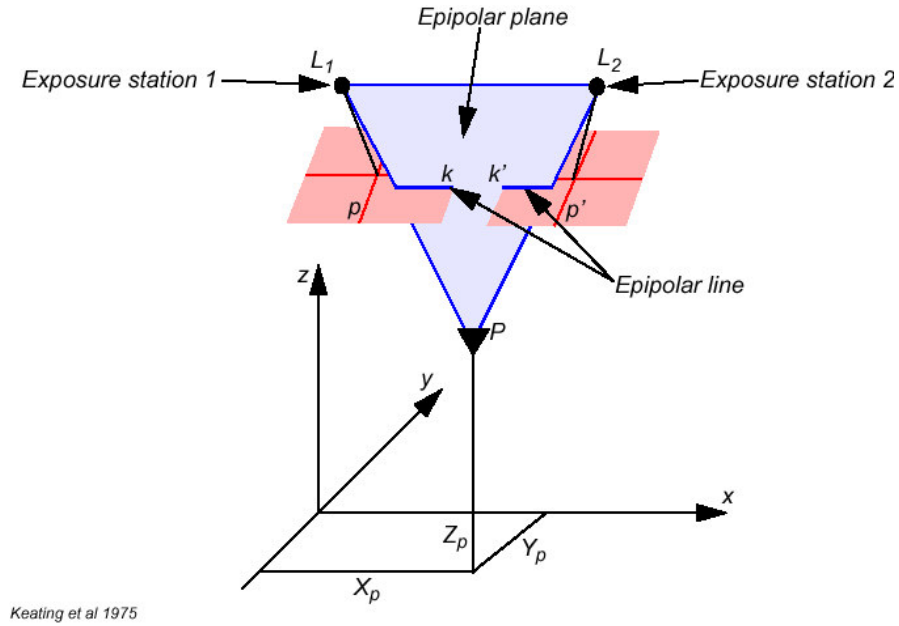
Fig 2.3: Epipolar geometry and the coplanarity condition

The search and matching process for digital image matching occurs along a straight line (i.e., epipolar line), thus simplifying the matching process. Figure 2.4 illustrates an image point on a reference image being located along the epipolar line of an adjacent overlapping image.
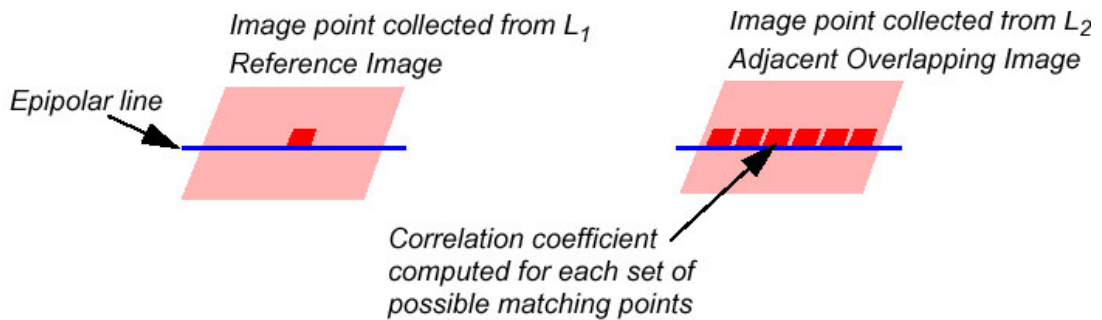
Fig 2.4: Matching image points

The epipolar constraint can only be applied if the image orientations and position of each sensor have been solved (ERDAS 2000). Epipolar images can minimizes the registration error in the y-direction (Olesonr, 2002).

With the aforementioned constraint, feature-based matching technique is used to determine the correspondence between two image features. Most feature-based techniques match extracted point features (this is called feature point matching), as opposed to other features, such as lines or complex objects. The feature points are also commonly referred to as interest points. Poor contrast areas can be avoided with feature-based matching. Another image matching technique, called least square matching, is used for the high accuracy of tie points.

The difference in location between the images gives the parallax, arising from the terrain relief, which is then converted to absolute elevation values above the local mean sea level datum using space intersection solution (Toutin, 2001).

Parallax, or elevation induced offset, for each pixel in the image is used to derive height information. Parallax is a function of both the difference in the two incidence angles (the angle between nadir and the path to the target area) and the local topography. An area with little elevation difference requires a large angle to produce the needed parallax. An area of great elevation difference requires a smaller angle (ERDAS 2001).

2.1.4.3 Space Forward Intersection Technique

Due to the time consuming and labor intensive procedures associated with collecting ground control, most photogrammetric applications do not have an abundant number of GCPs. Additionally, the exterior orientation parameters associated with an image are normally unknown. In this case, a photogrammetric technique called space forward intersection is used to define the variables required to perform in this task of DEM extraction.

Space forward intersection is a technique that is commonly used to determine the ground coordinates X, Y, and Z of points that appear in the overlapping areas of two or more images based on known interior and exterior orientation parameters. Using the collinearity condition, stating that the corresponding light rays from the two exposure stations pass through the corresponding image points on the two images, and intersect at the same ground point. Figure 2.5 illustrates the concept associated with space forward intersection (Erdas IMAGINE, 2001).
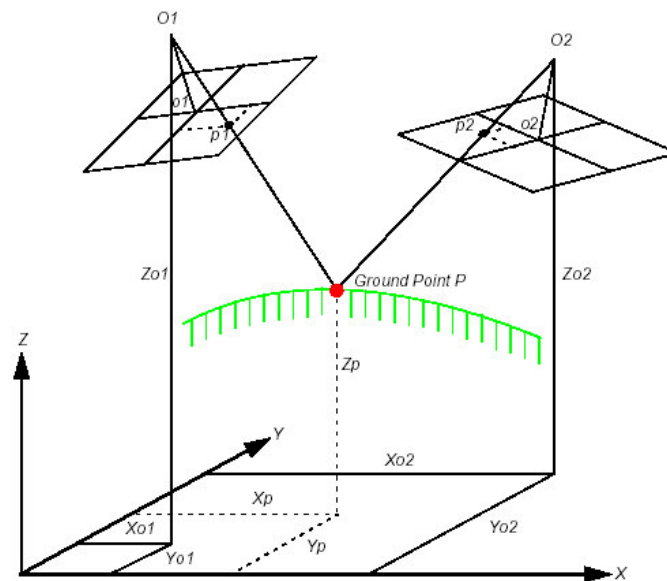
Fig 2.5: Space Forward Intersection

Space forward intersection techniques assume that the exterior orientation parameters associated with the images are known. Using the collinearity equations, the exterior orientation parameters along with the image coordinate measurements of point *p1* on image 1 and point *p2* on image 2 are input to compute the *Xp*, *Yp,* and *Zp* coordinates of ground point *P*. The positional elements of exterior orientation include *Xo1*, *Yo1,* and *Zo1 on image 1 and Xo2*, *Yo2,* and *Zo2 on image 2*. They define the position of the perspective centers (*O1 and O2*) with respect to the ground space coordinate system (*X, Y,* and *Z*). *Zo1 and Zo2* is commonly referred to as the height of the satellite above sea level, which is commonly defined by a datum.

The automatically extracted and calculated mass points (with x,y and z coordinates) are used as a basis for interpolating to construct a DEM.

2.2   Pushbroom Sensor Models

Sensors have perspective centers. The perspective center is the optical center of a sensor. All light rays that pass through a sensor pass through the perspective center. The positional elements of exterior orientation define the position of the perspective center relative to the ground coordinate system. Pushbroom data are collected along multiple scan lines, according to the number of scan lines in an image, with each scan line having its own perspective center.

As Figure 2.6 shows, pushbroom scanners record multispectral image data along a swath beneath a satellite. This system builds up a two-dimensional image by recording successive scan lines that are oriented at right angles to the flight direction. Linear arrays of detectors are used to record the reflected EM energy. A single array may contain over 10,000 individual detectors. Each spectral band of sensing requires its own linear array. Normally, the arrays are located in the focal plane of the scanner such that each scan line is viewed by all arrays simultaneously (Lillesand, 2000).
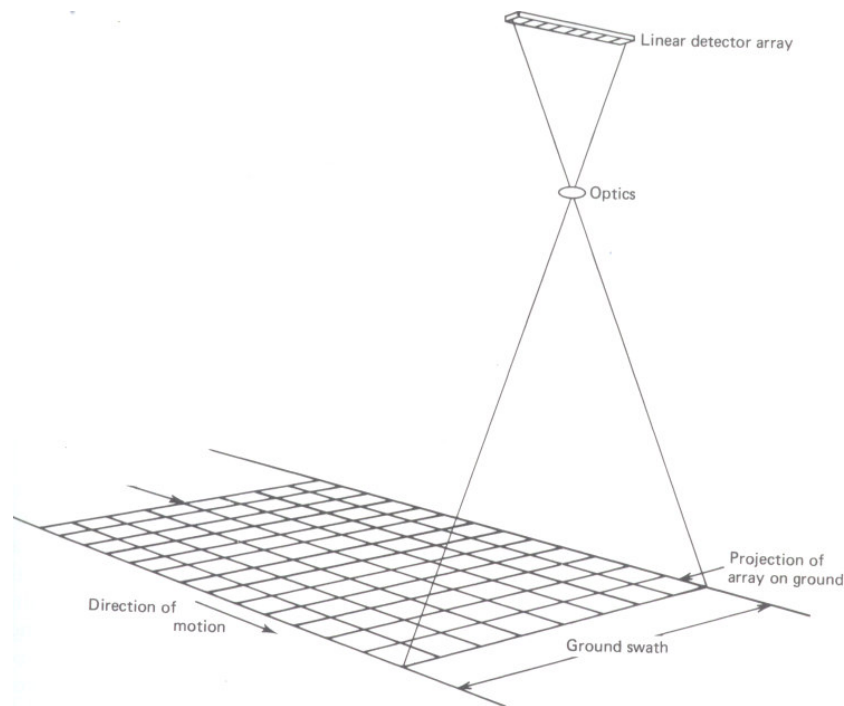
Fig 2.6: Pushbroom scanner system operation

As Lillesand (2000) indicates, linear array systems offer a number of advantages: 1) Linear arrays provide a longer dwell time for each detector to measure the energy from each ground resolution. This enables a stronger signal to be recorded and a greater range in the signal levels that can be sensed, which leads to better radiometric resolution. 2) The geometric integrity of linear array systems is great because of the fixed relationship among detector elements recording each scan line. Thus geometric errors by variations during the sensing process can be reduced. 3) Linear arrays are solid-state microelectronic devices, so less power is required for their operation due to the smaller size and weight. 4) Having no moving parts, a linear array system has higher reliability and longer life expectancy.

Nevertheless, pushbroom has also disadvantage: this system needs to calibrate many more detectors. In addition, linear array detectors that are sensitive to wavelengths longer than the mid-IR are not readily available currently.

The following geometric models are supported in Erdas IMAGINE OrthoBase pro:

Generic Pushbroom

This type of satellite pushbroom sensor can be used for satellites other than SPOT and IRS-1C, which scan along a line to collect data. Sensor model parameters associated with the internal geometry of the sensor must be provided.

In this study, the ASTER sensor is used. ASTER doesn't provide sensor model properties as SPOT and some other pushbroom sensors, thus the geometric model of the sensor has to be estimated in exterior orientation.

SPOT Pushbroom

The SPOT pushbroom sensor supports SPOT Panchromatic (10 meter ground resolution), and SPOT XS Multispectral (20 meter ground resolution) imagery. Sensor model properties associated with the satellite are automatically derived from the header file of the imagery for subsequent processing.

IRS-1C Pushbroom

The IRS-1C sensor model supports imagery collected from the IRS-1C pushbroom sensor model (5 meter ground resolution). Sensor model properties associated with the satellite are automatically derived from the header file of the imagery for subsequent processing.

2.3   Producing DEM Using Satellite Remote Sensing Data

Satellite imagery has a wide variety of implementation. High resolution images are lending themselves to all kinds of Geographical Information Systems (GIS) applications, ranging from asset and risk analysis, to investment, resource, transportation and logistics planning, as well as land use and policy development, cartography and telecommunication, etc.

Remote sensing stereo image pairs in digital format can be used to derive 3D terrain information similar to conventional photogrammetry, which is based on the use of analogue image pairs. There is a global chain to process stereo-digital data (http://dib.joanneum.ac.at/fe_serv/stereo_dem_gen.html):

- The geometric modeling, i.e. the determination and optimization of parametric imaging models for the stereo data;
- The automatic image correlation in order to find corresponding points in usually preregistered stereo images;
- The generation of a DEM through calculation of 3D coordinates and interpolation of regular elevation raster.

Examples of satellite imaging systems designed to provide either cross-track or along-track stereo data in digital formats include the High Resolution Visible (HRV) sensor of SPOT-1, -2, and –3, available since 1986, the Optical System (OPS) of the Japan Earth Resource Satellite (JERS-1) launched in 1992, the Modular Opto-Electronic Multispectral Scanner (second version) MOMS-02, flown on the German Spacelab D2 mission in 1993, and, most recently, the Pansensor aboard the Indian IRS-1C satellite. These digital systems have provided scientists with stereo image data with 4.5 m (MOMS) to 20 m (HRV) ground instantaneous field of view (GIFOV). Using these data, the feasibility of deriving elevations accurate to ±1 pixel or better by automated stereo correlation techniques has been demonstrated.

The following lists the main satellite data used for stereo-processing:

- ASTER image pairs
- SPOT Panchromatic image pairs
- IKONOS stereo imagery
- ERS SAR image pairs
- JERS inflight stereo data
- MOMS inflight stereo data
- IRS-1C stereo data
- Landsat TM and SPOT XS multisensor image pair
- SPOT XS multisensor image pair

- RADARSAT image pairs

2.3.1 SPOT

The French earth observation satellites SPOT-1, 2, 3 and 4 (Figure 2.7) were launched into a sun-synchronous sub-recurrent orbit at an altitude of about 822 km in 1986, 1990, 1993 and 1998 respectively. SPOT can observe not only the earth's surface just underneath the satellite but also slantwise to the satellite's path by changing the scan direction of the sensors. It can shorten the time period for observing a specified area repetitively.

Fig 2.7: SPOT Satellite

SPOT-1, -2 and −3 are equipped with CCD sensors called High Resolution Visible Imaging System (HRV). SPOT −4 is equipped with two CCD sensors, HRV's successor, High Resolution Visible and Infrared (HRVIR) and Vegetation (VGT).

The observation bands of HRVIR are basically the same as HRV and the newly added band 4, short wave infrared (SWIR: 1.58 to 1.75Vm). The VGT sensor observes wide area with a swath of 2,250 km.

A SPOT stereo pair can be acquired for example by panchromatic images (Spot 1, 2, 3) or multispectral images (three-band or four-band). This yields relief for mapping at scales of 1:200,000, 1:100,000, 1:50,000 or 1:25,000. In fact, the SPOT Image archives hold thousands of stereo pairs from around the world. These can be produced in both a digital format as well as photographic form.

2.3.2 IKONOS

Launched in September 1999, IKONOS 2 is a commercial satellite, owned and operated by Space Imaging (Figure 2.8). The satellite can acquire multispectral images with high resolutions. IKONOS 1-meter resolution Panchromatic, 1-meter resolution Pan-sharpened Multispectral and 4-meter resolution Multispectral (color) products can be used for a wide variety of applications and represent one of the highest resolution satellite imageries currently commercially available. The satellite carries

a state-of-the-art sensor and is one of the most advanced commercial imaging system currently in orbit (http://www.geosig.com/ptsatellite.htm). Conventional space borne optical platforms have resolution on the order of 30 metres, making their data useless for deriving maps of a rapidly varying region, such as an urban area. IKONOS, on the other hand, has resolutions of up to one metre, which are more or less commensurate with the variations encountered in urban applications.
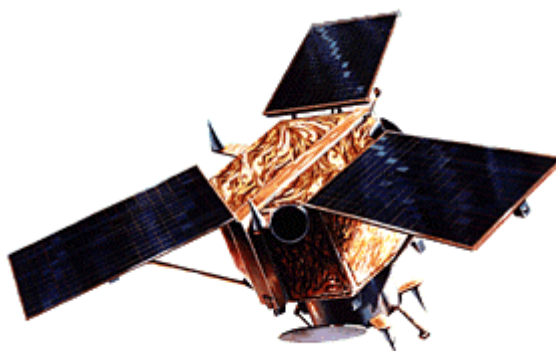
Fig 2.8: Artist's impression of the Ikonos satellite
(provided by http://www.met.ed.ac.uk/~alastm/spec.html)

The same as for other satellite stereo-data, in order to accurately create or extract geographic information from raw IKONOS imagery, the image geometry model (IGM) must be included with the imagery. The IGM consists of several metadata files. The metadata files contain RPCs (rational polynomial coefficients), which are a series of coefficients used to describe the relationship between the image as it existed when captured and the Earth's surface. With the availability of RPCs, the IKONOS imagery can be used to accurately create orthorectified images, digital stereo models (DSMs), and DEMs without the need for ground control points (GCPs). If a higher degree of accuracy is required for a specific mapping project, the RPCs can be refined using GCPs.

2.3.3 ERS

The European Remote Sensing Satellites (ERS-1 and ERS-2, launched by European Space Agency in 1991 and 1995 respectively) orbit the Earth in about 100 minutes and in 35 days they have covered nearly every corner of the globe at least once. One important instrument for our coal fire project is the Synthetic Aperture Radar (SAR). When two consecutive images are merged through the technique of interferometry (INSAR), the instrument can even detect elevation changes in the order of centimeter over an approximately 100x100 km area. The ERS data will also be used for land subsidence assessment by means of differential interferometry.

A DEM covering the Xinjiang and Ningxia coal fire areas has already been produced using ERS data, with 20m resolution.

2.3.4 Space Shuttle

The Shuttle Radar Topography Mission (SRTM) data products result from a collaborative mission by the National Aeronautics and Space Administration (NASA), the National Imagery and Mapping Agency (NIMA), the German space agency (DLR) and Italian Space Agency (ASI), to generate a near-global digital elevation model (DEM) of the Earth using radar interferometry.

The SRTM data flight occurred Feb. 11-22, 2000 on STS-99 and successfully fulfilled all mission objectives. Following a lengthy calibration and validation phase, the 12 terabytes of raw data are currently being processed into digital elevation maps (Letham, 2002).

Displaying spectacular new 3-D images and animations of California from space, scientists at NASA's Jet Propulsion Laboratory, Pasadena, Calif., recently announced the release of high-resolution topographic data of the continental United States gathered during the February 2000 Shuttle Radar Topography Mission -- a mission that is creating the world's best global topographic map (Figure 2.9).
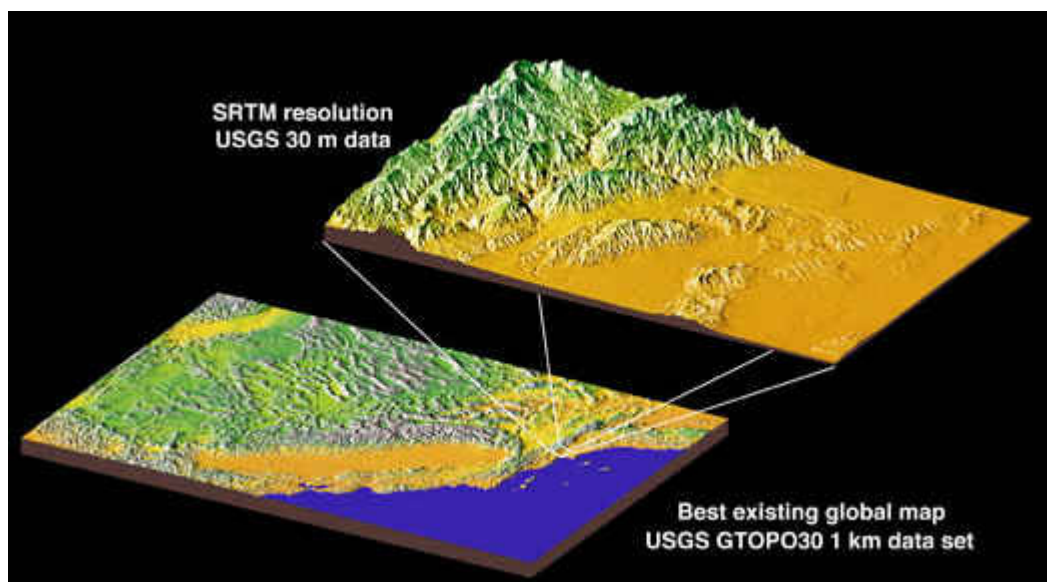
Fig 2.9: SRTM data compared to GTOPO30

About the SRTM Mission

The Shuttle Radar Topography Mission was flown aboard Space Shuttle Endeavour February 11-22, 2000. It used modified versions of the same instruments that comprised the Space Shuttle Imaging Radar-C/X-Band Synthetic Aperture Radar that flew twice on Endeavour in 1994.

The mission collected 3-D measurements of Earth's land surface using radar interferometry, which compares two radar images taken at slightly different locations to obtain elevation or surface-change information. To collect the data, engineers added a 60-meter (approximately 200-foot) mast, installed additional C-band and X-band antennas, and improved tracking and navigation devices.

The Shuttle Radar Topography Mission supports NASA's Earth Science Enterprise, Washington, D.C., a long-term research and technology program designed to examine Earth's land, oceans, atmosphere, ice and life as a total integrated system (http://spatialnews.geocomm.com/features/srtm_jan2002/).

2.4   Using ASTER Image Pair to Extract DEM

For the studies of the earth observations and researches, DEM dataset from satellite imagery is useful. SPOT and aerial photography have been used for many detailed site specific studies. However, they are pretty costly. ASTER stereo imagery is now being acquired and it is hoped that, throughout it's 5 year mission, most of the earth's land surface will be imaged in stereo. It provides a major data source for generating high resolution DEMs for most part of the world at a relatively low cost (Davis, 2001).

ASTER (Advanced Spaceborne Thermal Emission and Reflection Radiometer) (Figure 2.10), provided by the Ministry of International Trade and Industry (MITI), Tokyo, Japan, is a high spatial resolution imaging instrument that is flying on the Terra platform of EOS-AM1 polar orbiting spacecraft from 1998. The base-to-height (B/H) ratio, i.e. geometric stereo disposition, is about 0.6 and an intersection angle (off-nadir) is about 27.7 degrees. The ground-instantaneous-field-of-view (GIFOV) for ASTER stereo data is 15 m over a 60 km swath width. This research facility instrument covers a wide spectral region from visible to thermal infrared, with 14 spectral bands of high spatial, spectral and radiometric resolution.
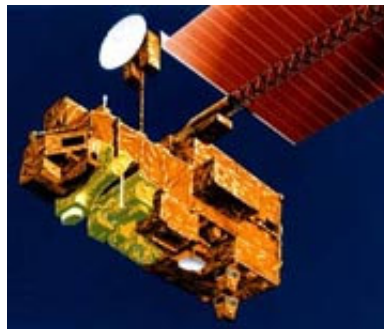

Fig 2.10:   ASTER Satellite (provided by http://asterweb.jpl.nasa.gov)

This advanced multispectral sensor monitors the Earth with three different subsystems: the Visible and Near Infrared radiometer, the Shortwave Infrared radiometer and the Thermal lnfrared radiometer (Table2.1).

Subsystem	Band No.	Spectral Ranges (µm)	Spatial Resolution	Signal Quantization Levels
VNIR	1 2 3N 3B	0.52-0.60 0.63-0.69 0.78-0.86 0.78-0.86	15m	8 bits
SWIR	4 5 6 7 8 9	1.600-1.700 2.145-2.185 2.185-2.225 2.235-2.285 2.295-2.365 2.360-2.430	30m	8 bits
TIR	10 11 12 13 14	8.125-8.475 8.475-8.825 8.925-9.275 10.25-10.95 10.95-11.65	90m	12 bits

Stereo Base-to-Height Ratio	0.6 (along-track)
Swath Width	60 km
Total Coverage in Cross-Track Direction by Pointing	232 km

Table 2.1: Aster Baseline Performance Requirements

Because the data have a wide spectral coverage and relatively high spatial resolution, users are able to discriminate a variety of surface materials and reduce problems in some lower resolution data resulting from mixed pixels.

The primary science objective of ASTER mission is to improve understanding of the local- and regional-scale processes occurring on or near the earth's surface and lower atmosphere, including surface-atmosphere interactions. Specific areas of the science investigation include the following (Yamaguchi, 1998):

1. Land surface climatology;
2. Vegetation and ecosystem dynamics;
3. Volcano monitoring;
4. Hazard monitoring;
5. Aerosols and clouds;
6. Carbon cycling in the marine ecosystem;
7. Hydrology;
8. Geology and soil;
9. Land surface and land cover change.

Due to the high data rate of the three ASTER imaging subsystems, only eight minutes of data are acquired per orbit, and the along-track stereo imaging is then favored. The visible and near infrared radiometer is useful in assessing vegetation and iron-oxide minerals in surface soils and rocks. It is

especially useful for topographic interpretation because it has along-track stereo coverage in band 3, with nadir and backward views with 15 m spatial resolution.

The nadir-backward stereo-viewing geometry (Figure 2.11) potentially gives a higher probability of obtaining a cloud-free image pair, as compared to a side stereo observation system requiring multi-orbit observation, such as the SPOT HRV (Yamaguchi, 1998).

Band 3 (Aft)   **Band 3 (Nadir)**   **Orbit path**

Surface
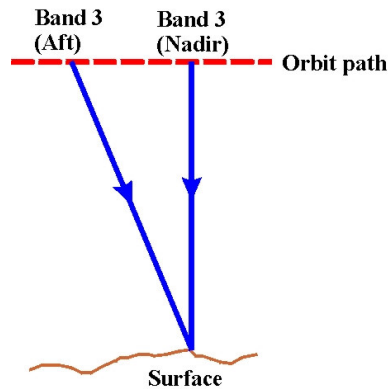
Fig 2.11: Simplified sketch diagram showing along track stereo geometries
(diagram not drawn to scale, provide by Davis A.M.)

The ASTER Science Team provides data products for multi-application. The list is shown as Table 2.2:

Product code	Product name
1A	*RECONSTRUCTED, UNPROCESSED INSTRUMENT DATA*
2B	Radiance at sensor
2A01	Brightness temperature at sensor
2A02	Relative spectral emissivity (D-stretch)
2A03	Relative spectral reflectance (D-stretch)
2B01	Surface radiance
2B03	Surface temperature
2B04	Surface emissivity
2B05	Surface reflectance
4A	Polar cloud map (after launch)
4A21	Digital elevation mode (absolute)
3A01	Radiance at sensor with ortho-photo correction
4A01	*DIGITAL ELEVATION MODEL (RELATIVE)*

Table 2.2: ASTER Standard (1A to 4A21) and Semistandard (3A01 and 4A01) Data Products

ASTER products have the following characteristics that are an improvement over past remote sensing products:

- A wider spectral range and a higher spectral resolution are offered covering the spectral range of 0.52 to 11.65 microns with 14 bands.
- 15m, 30m, and 90m spatial resolutions are offered in the visible and near infrared spectral region, the shortwave infrared spectral region, and the thermal infrared spectral region, respectively.
- For band 3 (0.76 microns to 0.86 microns), both the usual nadir-looking telescope and a backward-looking telescope are used to produce stereoscopic images acquired in the same orbit.

The Japanese are responsible for providing ASTER Level 1 data products. ASTER instrument has two types of Level-1 data, Level-1A and Level-1B. Level-1A data are formally defined as reconstructed, unprocessed instrument data at full resolution. According to this definition, the ASTER Level-1A data consist of the image data, the radiometric coefficients, the geometric coefficients, and other auxiliary data, without applying the coefficients to the image data to maintain the original data values. The Level-1B data are generated by applying these coefficients for radiometric calibration and geometric resampling. All acquired image data are required to be produced to Level-1A. A maximum of 310 scenes per day are to be processed to Level-1B data in response to requests from users.

ASTER Digital Elevation Model is a product that is generated from a pair of ASTER Level 1A images (see Table 2.3). This Level 1A input includes bands 3N (nadir) and 3B (aft-viewing) from the Visible Near Infra-Red telescope's along-track stereo data that is acquired in the spectral range of 0.78 to 0.86 microns. ASTER DEMs can be generated either with or without ground control points (GCPs). An Absolute DEM is created with GCPs that are supplied by an end-user who has requested the product. These DEMs have an absolute horizontal and vertical accuracy of up to 7 meters with appropriate GCPs and up to 10 meters without GCPs. Alternatively, a Relative DEM can also be generated without GCPs.

Unit of Coverage:	60km**x**60km ASTER Scene		
Format:	Data consist of a regular array of elevations (in metres) referenced to either the lowest elevation in the scene ("relative DEM") or the mean sea level ("absolute DEM") and projected in the Universal Transverse Mercator (UTM) coordinate system.		
Resolution:	1. x-y, 30 m (posting) 2. z, 1 m (smallest increment)		
Product Name	# of GCPs (Minimum)	GCPs ($RMSE_{xyz}$) Accuracy	DEM ($RMSE_{xyz}$) Accuracy
Relative DEM	0	N/A	10-30 m
Absolute DEM	1	15-30 m	15-50 m
Absolute DEM	4	5-15 m	7-30 m

Table 2.3: Definitions/Specifications for Standard ASTER DEM Data Products

These DEMs can be used to derive absolute slope and slope aspect which is good up to 5 degrees over a horizontal distance of over 100 meters. ASTER DEMs are expected to meet map accuracy standards for scales from 1:50,000 to 1:250,000.

DEM extraction from ASTER stereo images is based on the principle of automatic stereo correlation techniques. The accuracy to which absolute elevations can be derived by those photogrammetric techniques is governed by: 1) B/H ratio, 2) reliability of the correlation procedure, and 3) accuracy and density of ground control points.

As Angela Altmaier (2002) analyzed, the DEM accuracy depend mainly on the following factors: sensor model, image deformations, geometric accuracy and resolution of scanner as well as accuracy of interior orientation. Furthermore, the number, accuracy and regular horizontal and vertical distribution of the GCPs are important.

According to Roy Welch (1998), height differences (Δh) or relative elevations of objects are closely approximated by the following equation (see Figure 2.12):

$$\Delta h \approx \Delta p \, / \, \tan\alpha \approx \Delta p \, / \, (B/H).$$

Where the angle α is formed between the vertical axis from the nadir camera (3N) at observation station 1 and the intersecting ray from the backward pointing camera (3B) at observation station 2. This angle yields a B/H ratio of 0.6 for ASTER. The difference in parallax (Δp) is computed from the stereo correlation procedure, and it is proportional to the terrain elevation relative to the vertical datum. The ability to control the parallax error depends on the availability and accuracy of ground control points (Yamaguchi, 1998).
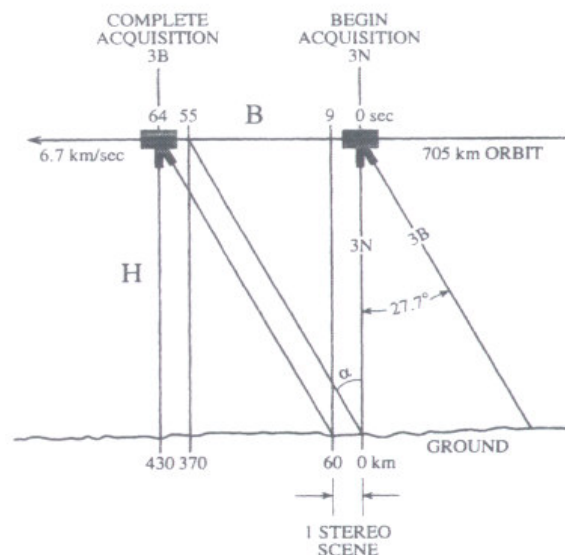
***Fig 2.12: Simplified Diagram of Imaging geometry and Data Acquisition timing
for ASTER Along-track Stereo***

These relative height measurements can be transformed to absolute elevations tied to a vertical datum by employing an adequate number and distribution of GCPs. Such GCPs can be obtained from existing large-to-medium scale topographic maps or from Global Positioning System (GPS) surveys.

Currently, ASTER team is carrying out a six-year mission to acquiring coherent, digital, cloud-free global coverage of the earth's land surface by the along-track stereo imager instrument. The system is configured to acquire data with a base-to-height ratio of 0.6 at 15 m spatial resolution and can acquire 50,700x600 km stereo pairs per day. The specific objective of the ASTER stereo experiment are: 1) to acquire cloud-free stereo coverage of 80% of the land surface between 85º N and 85º S and 2) to produce, with commercial software, standard product DEMs at a rate of one-per-day starting at launch.

3. Methodology

3.1 Available Data

There are some materials provided for this study (Table 3.1). Other than original data sources, some ancillary data was also used for this research.

Material Name	Data Description	Producing or Acquisition Date	Remark
ASTER L1A Image Pair	VNIR Band 3 nadir-backward views, spatial resolution 15 m	August, 2001 (acquisition date)	1)The main data source of this study. 2)Some parts with cloud / shadows
Russian Topographic Map	Scale: 1:100,000, contour interval 20 m, coordinate system: UTM/WGS 84	1978 (producing date)	Due to the old production time of this map, latest ground truth data is needed
Ancillary Data: ASTER L4 DEM (Absolute)	Spatial resolution 30m, produced by ASTER Science Team, coordinate system: UTM/WGS 84	April, 2001 (acquisition date)	1)As a reference for GCPs measurement and accuracy assessment. 2)Unedited, intended for ground-truth evaluation: containing numerous voids (Figure 3.1).
Ancillary Data: Multispectral ASTER Image	ASTER Band 1,2,3 data, false color, with coordinate system: UTM/WGS 84	August, 2001 (acquisition date)	As an overlay on the final DEM for visual representation.

*Table 3.1: Available data for DEM extraction of this study*
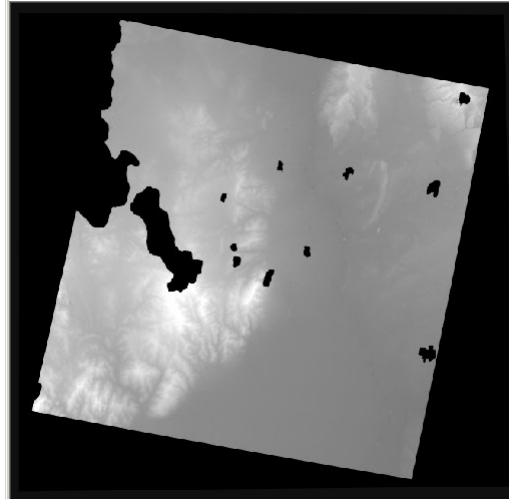
Fig 3.1: ASTER L4 DEM provided by ASTER Science Team

3.2   Software

- ERDAS IMAGINE 8.5, digital image processing software. This version supports the *pushbroom (along-track)* sensor model. For this study, the main software is OrthoBASE pro, which supports various camera/sensor models to extract a DEM and generate ortho-rectified images. Other modules include Virtual GIS, Stereo Analyst, DataPrep, Viewer and Import, for helping creating, modifying and presenting the DEM extracted.

- ArcView GIS 3.2, with "3D Analyst" extension. This is a product of Environmental Systems Research Institute Inc. It is a Geographic Information System (GIS) software, which can visualize, explore, query and analyze data spatially. This study uses this software to help performing 3D modeling and 3D analyzing.

3.3   Analysis of the Methodology

The methodology adopted in this research can be presented as:

- ASTER nadir and backward looking image data can be obtained associated with metadata, which can be interpreted to obtain the interior orientation parameters;
- Combine the data collected from topographic maps, such as contour lines and spot height measurements, with GPS measurements from the field work to precisely measure GCPs for exterior orientation of the satellite images;
- Automatic extraction of DEM with Erdas Imagine 8.5 and ArcView GIS 3.2, associated with related 3D modeling process of interpolation; proper modification and accuracy assessment;

- The final DEM obtained is used in the resampling process to generate the ortho-image, furthermore, output the derived products such as slope angle and aspect maps.

3.3.1   Internal Sensor Modeling

In order to process various Remote Sensing data, the model associated with a camera or a sensor must be defined first. This procedure includes the internal and external information input. In this case, the geometric modelling is referred to as "internal sensor modelling" using a generic pushbroom sensor having a perspective center for each scan line, as compared with the model definition of cameras having one perspective center, which is referred to as "interior orientation" (ERDAS, 2001).

A metadata associated with the ASTER image pair used in this study provides the internal parameters for this generic pushbroom model. A referential parameter dataset, offered by Geosystems (www.geosystems.de), as given in Table 3.2 was used.

GENERAL		
Sensor name	ASTER VNIR Nadir	ASTER VNIR Backward
Focal length (mm)	329.0	329.0
Principal point x0 (mm)	0.0	0.0
Principal point y0 (mm)	0.0	0.0
Pixel size (mm)	0.007	0.007
Sensor columns	4100	5000
MODEL PARAMETERS		
Polynomial Orders of Sensor Model		
X	2	2
Y	2	2
Z	2	2
Omega	1	1
Phi	1	1
Kappa	2	2
SPECIFIC		
	ASTER VNIR Nadir	ASTER VNIR Backward
Side incidence (degrees)	-8.586	-8.586
Track incidence (degrees)	0.0	-30.96
Ground resolution (meters)	15.0	15.0
Sensor Line Along Axis	Y	Y

Table 3.2: ASTER Model Used for Internal Sensor Modelling

Some parameters are used especially for pushbroom sensors:

X, Y, Z:

This is the coordinates of the exposure location.

Omega, Phi, Kappa:

This is the rotation system defining the axis used to characterize the orientation of a sensor at the time of exposure. An omega rotation is around the x-axis, phi rotation around the y-axis, and kappa rotation around the z-axis.

Side Incidence (degrees):

This is the angle between the vertical position of the satellite and the side viewing direction of the satellite when the sensor is scanning along the side.

Track Incidence (degrees):

This is the angle between the vertical position of the satellite and the forward or backward viewing direction of the satellite.

Sensor Line Along Axis:

This defines the direction of the scan line which is used by the satellite to record the data. Each scan line has a perspective center with six exterior orientation parameters including X, Y, Z, omega, phi, and kappa. If ground-based images are used, the image direction is the Y-axis.

For generic pushbroom model, the "track incidence" and "sensor line along axis" are additional options, relative to other pushbroom models.

The exterior orientation specification are input as model parameters in this stage, i.e. the "polynomial orders", which describes the sensor orbit. One-dimensional polynomial models are used to define the position and orientation of the sensor as they existed at the time of capture. After triangulation has been performed, polynomial coefficient are calculated. The number of coefficients calculated is determined by the polynomial orders. The number of polynomial parameters (NOPP) increases with the order of the polynomial (OP) (NOPP = OP + 1) (GEOSYSTEMS, 2002). Thus in this case we have 32 unknown sensor parameters according to Table 3.2. The exterior orientation parameters will be computed based on measured GCPs, and are provided in the triangulation report afterwards.

3.3.2   Exterior Orientation

Exterior orientation is the position and orientation of the exposure stations for the images.

In this case, the exterior orientation values will be calculated based on the measurement of GCPs. This step is the key for the DEM extraction from ASTER image pair. In fact, in many actual photogrammetric tasks, the achievements can be reliable mainly on the basis of the quality of ground control points used.

The measurement of ground control points needs to be accurate, sufficient and evenly-distributed. Combining with the GCPs data obtained from the fieldwork, and supplementary points measured from the available topographic map, an automatic procedure of tie points collection is performed on the basis of digital image matching. Tie point measurement results in a relative orientation on both images; while GCPs measurement results in an absolute orientation to the ground-truth.

Collection of GCPs

A minimum of 3 control points are theoretically sufficient; while one single ground control point determines 4 unknown parameters, as we have 32 unknown sensor parameters, there are at least 8 "full" ground control points needed given the absence of tie points. However, in order to increase the positioning accuracy, to detect gross errors, and finally to enhance the statistical meaning of the resulting accuracy values after triangulation, more control points have to be collected to get reliable estimates of the quality of the results. In fact, appropriate amounts of control points enable quality control and make it easier to detect blunders. In this case, 54-74 "full" GCPs (x, y, z) are suggested, depending on the number of model parameters' polynomial order, including at least 4 in the corners of the overlapping area (GEOSYSTEMS, 2002).

Good GCP locations are clear-defined ground points covering all kinds of terrain. The following features on the Earth's surface are commonly used as GCPs: intersection of roads; utility infrastructure (e.g., fire hydrants and manhole covers); intersection of agricultural plots of land. GCPs should be collected at the high and low elevations, to avoid planimetric and elevation extrapolations (Toutin, 2001).

Moreover, the effect of the automatic error detection depends not only on the mathematical model, but also depends on the redundancy in the block. Therefore, more tie points in more overlap areas contribute to better gross error detection. In addition, inaccurate GCPs can distribute their errors to correct tie points; therefore, the ground and image coordinates of GCPs should have better accuracy than tie points (Erdas, 2001). This precise point accuracy will contribute to improving the interior orientation and the exterior orientation afterwards (Altmaier, 2002).

Next, the mathematical relationship between the images, the sensor model, and the ground can be defined. This "triangulation" process using "space forward technique" as the functional model (ERDAS, 2001), simultaneously estimates:

- The position (X, Y, Z) and orientation (omega, phi, kappa) of each image as they existed at the time of image capture (exterior orientation parameters).
- The x, y, and z coordinates of tie points.
- The internal sensor modelling parameters, the geometric errors associated with the sensor are considered.
- Systematic error.

The result of point measurement should be checked including:

- The distribution of generated tie points are covering the main part of the image;
- The elevations of automatically generated tie points can match the features on the image, i.e. mountainous regions, plain regions, etc.;
- Manually modify some "error points", or delete them.

3.3.3 DEM Extraction

There will be two types of DEM models derived (referenced to section 2.1.3): raster DEM and vector implementation of 3D surfaces TIN, for different interested applications of further study.

Several interpolation methods involved need to be considered for the DEM extraction:

A nearest-neighbour interpolation helps to retain the original pixel values in the output image; while the other techniques such as linear, bilinear or bicubic interpolation tend to smooth the image and subdue some locally interesting features which have high spatial frequency.

There are four interpolation methods available to create gridded surfaces: Inverse Distance Weighted (IDW), spline, kriging, and polynomial trend. Each method has different characteristics that make them appropriate for different source data and applications. (Esri, 2002)

*Inverse Distance Weighted (IDW):*This interpolator assumes that each input point has a local influence that diminishes with distance. It weights the points closer to the processing cell greater than those farther away. A specified number of points, or optionally all points within a specified radius, can be used to determine the output value for each location. Use of this method assumes that the variable being mapped decreases in influence with distance from its sampled location.

Spline: This interpolator is a general-purpose interpolation method that fits a minimum-curvature surface through the input points. Conceptually, it is like bending a sheet of rubber to pass through the points, while minimizing the total curvature of the surface. It fits a mathematical function to a specified number of nearest input points, while passing through the sample points. This method is best for gently varying surfaces such as elevation, water table heights, or pollution concentrations. It is not appropriate if there are large changes in the surface within a short horizontal distance, because it can overshoot estimated values.

Kriging: This interpolator assumes the distance or direction between sample points reflects spatial correlation that can be used to explain variation in the surface. Kriging fits a mathematical function to a specified number of points, or optionally all points within a specified radius, to determine the output value for each location. The use of kriging involves several steps: exploratory statistical analysis of the data, variogram modeling; then creating the surface and analyzing its optional variance surface. This function is most appropriate when you know there is a spatially correlated distance or directional bias in the data. It is often used in soil science and geology.

Trend: This interpolator fits a mathematical function, a polynomial of specified order to all input points. When calculating the mathematical function to describe the resulting surface, Trend uses a least-squares regression fit. The resulting surface minimizes the variance in relation to the input point values. That is, at all the known input points, when adding up the difference between the actual values and the estimated values, the variance will be the smallest possible. The resulting surface will rarely go through the known input points.

3.3.4 Assessment Ways

According to the actual conditions of acquiring related referential data, there will be some appropriate methods used in the accuracy assessment in this study:

1) Overlay the orthoimage on the DEM to compare the terrain relief and the features;

2) Overlay the DEM on the topographic map to compare the features;

3) Overlay the derived contour map after DEM extraction on the original topographic map;

The above-mentioned assessment methods will be used for general evaluation, the main task is to check the conformance of the computed terrain relief and the original features on both extracted DEM and input data source.

4) Comparing with checkpoints; Freely choosing some points within the extent of the topographic map as the DEM checkpoints. The selection criteria should include all kinds of terrain characteristics, for example, mountain summits, slope surface, flat area, etc.

5) Comparing with other control; Some creditable control covering the common area, for example the ASTER L4 DEM provided by the ASTER Science Team, can be used as reference to check the accuracy of derived DEM in this study.

Theoretically, when figuring out the accuracy assessment, many factors must be considered: coordinates transformation, geometric correction, selection precision of check points, the accuracy of the materials used to collect the check points, and so on.

3.4 Accuracy Prediction

Depending on the types of collecting sources, GCPs can be measured on different precisions:
• Theodolite survey (millimeter to centimeter accuracy)
• Total station survey (millimeter to centimeter accuracy)
• Ground GPS (centimeter to meter accuracy)
• Planimetric and topographic maps (accuracy varies as a function of map scale, approximate accuracy between several meters to 40 meters or more)
• Digital orthorectified images (X and Y coordinates can be collected to an accuracy dependent on the resolution of the orthorectified image)
• DEMs (for the collection of vertical GCPs having Z coordinates associated with them, where accuracy is dependent on the resolution of the DEM and the accuracy of the input DEM)—(Erdas, 2001)

The theoretical accuracy of DEM is defined by next equation (Tokunaga, 1996):
Accuracy = (Ground Resolution)/(base and height ratio)* (matching Accuracy)
The ground resolution of ASTER image is 15m, and B/H=0.6. When there is no error at orientation elements and stereo matching, the precision of DEM is decided by B/H and ground resolution. This is an ideal situation thoeretically, for example if the matching accuracy is around one pixel, the accuracy of the DEM can be around 25 meters.

Due to 1)the dated topographic map in a scale of 100,000 that is the main surface data source used in this study;
    2)the image pair that has some low-correlation parts, cloud and shadow covering parts;
the accuracy of this research could be impacted.
However, the accuracy based on the comparison between the computed elevations and the input z values, within the study area, should be acceptable using appropriate methodology.

4. DEM Extraction from ASTER Image Pair

4.1 Field Surveying

The fieldwork started on 5th September, 2002. For surveying, a mobile GPS receiver was used ("Garmin 3", 12XL). The planimetric accuracy is ±10m, less than an ASTER pixel used for DEM extraction; while altimetric accuracy is up to ±50m.

The ground control points (GCPs) were pre-defined on clear intersections of roads, streets, road—channel crossings, and some incised valleys on the map. By interpreting the ASTER image and the topographic map, some suitable points, existing both on the image and the map, were found.

The GPS receiver was used to:

1) Help to quickly find out the GCPs predefined, simultaneously observing the terrain characteristics to check the intepretation;

2) Compare with the x, y coordinates of the GCPs on the topographic map, if the difference is within the tolerance—in this case set to 30m since the 100,000 topographic map has a planimetric reading-error range of ±10 meters and considering GPS reading precision----the GCPs can be recorded with x, y and z values ("full" type GCPs) read from the topographic map, otherwise defined them as "vertical" control points because the exact positions could not be determined accurately but the z value by the aid of the topographic map representing the area.

For the field work, checklist sheets were designed for recording the ground control points. In the field, they were filled in as Table 4.1 shows:

GCP Checklist

Date & Time: **11/09/02 09:32**   Serial No: **2**

Code of Point on Map: 3					
Code of Point on Image: 3					
UTM/ WGS84	GPS Coordinates		Lat/Long	GPS Coordinates	
	648125E	4370978N		106°43'20"E	39°28'32"N
GPS	Altitude: 1175m				
Map	Elevation: 1120m				
EPE(Estimate of Position Error): 4m					
No.s of Satellites: 10					
Description (positions on the map): The intersection of railway and high way on the south of Wuda					
Terrain Type: Relatively flat, rare grass and low terrain					
Remarks: This cross is quite clear on both map and image					

Table 4.1: The sample of the Checklist for the field work

Due to the dated topographic map, which was produced in 1978, it was difficult to find as many clear control points as are shown on the map: the present settlements and infrastructure (roads, highways, etc.) have changed a lot. Additionally, it was impossible to travel all over the image area, such as mountainous regions, or very far from the coal fire field. During the fieldwork referential information was collected, such as the history of roads changes, data of some geodetic points, and so on. Finally, 48 good-quality control points were selected, among them 30 "full" and 18 "vertical" points.

In fact, visiting every location shown on the image is difficult and expensive. The GCPs collected from fieldwork will be input as sample data, and post-processing using appropriate interpolation method(s) is performed to estimate unknown positional coordinates.

4.2   DEM Extraction

The procedure of DEM extraction was mainly manipulated following linear workflow offered by IMAGINE OrthoBASE pro.

During the actual data processing of exterior orientation stage, GCPs quality affected the results considerably. In principle, the GCPs should be collected including both the image boundary areas and in the middle of the image, horizontally and vertically regularly distributed.

For optimally restoring the geometric model of the sensor, the GCPs measurement ultimately determines the DEM extraction results. It is necessary to use extra sources to supplement inadequate GCPs.

Acquiring extra data

An ASTER L4 DEM covering this image area was used to give extra coordinates other than the field extent. The ASTER L4 DEM has a spatial resolution of 30m, geographic coordinate system is UTM/WGS 84, the theoretical absolute horizontal and vertical accuracy is up to 10 meters without GCPs (http://edcdaac.usgs.gov/aster/ast14dem.html). At this stage, geocorrecting this DEM using GCPs was performed to make the data usable.

As an aid of reading extra data, a prompt ortho-image was generated using the triangulation achievement from those 48 GCPs. This ortho-image was assessed next by checking the conformance of terrain features between the topographic map and the ortho-image. It was found that the x, y positions of the image were quite accurate.

Thus, extra data were read from aforementioned resources. They were used to control the distortion and displacement of the computed sensor model.

Finally, there were 52 extra points selected in order to meet the input requirements: sufficient and accurate Ground Control Points (GCPs), evenly distributed on the image, along the boundary and in the corner-edges of the image (Figure 4.1).
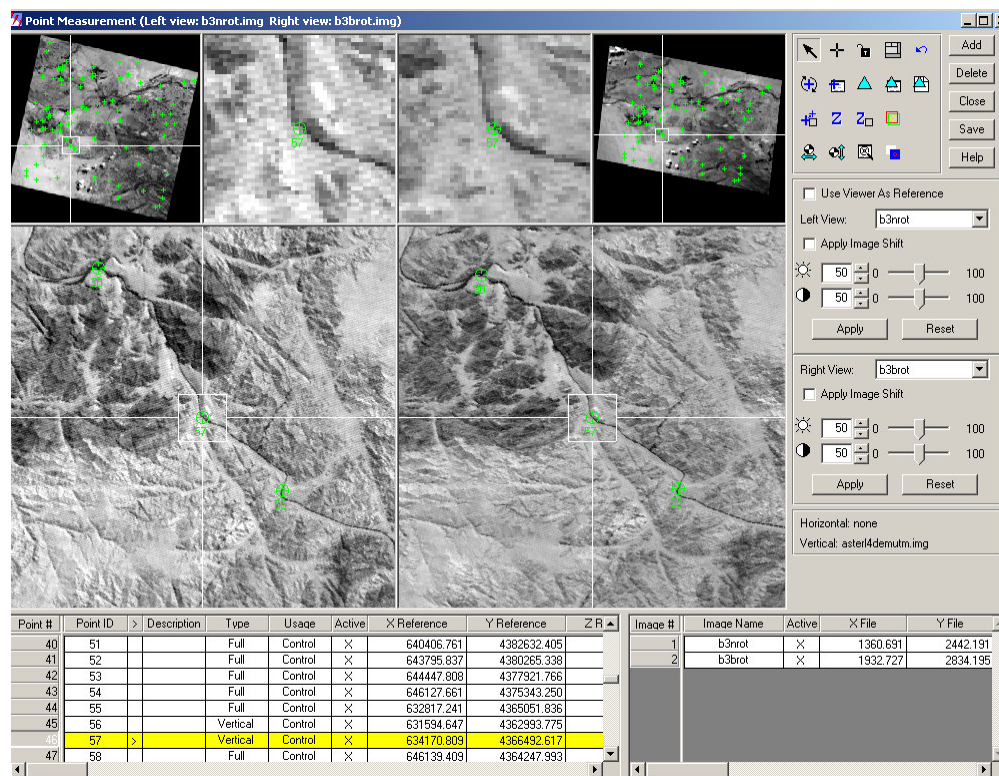
Fig 4.1: The distribution of control points on the image pair

In this exterior orientation, 100 control points were finally determined, among them 48 are from the field, and 52 from other data sources.

By setting Automatic Tie Point Generation Properties (Figure 4.2), and manually identifying tie points, a total of 312 tie points were generated (Figure 4.3).
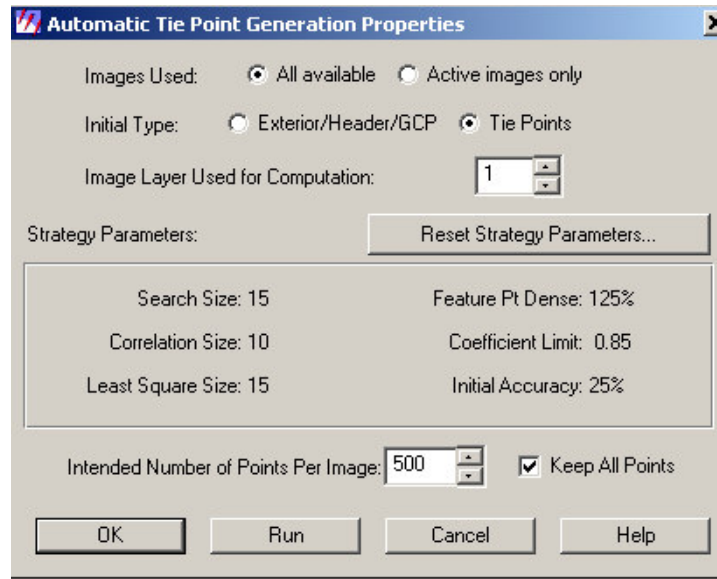
Fig 4.2: The strategy parameters for automatic tie generation
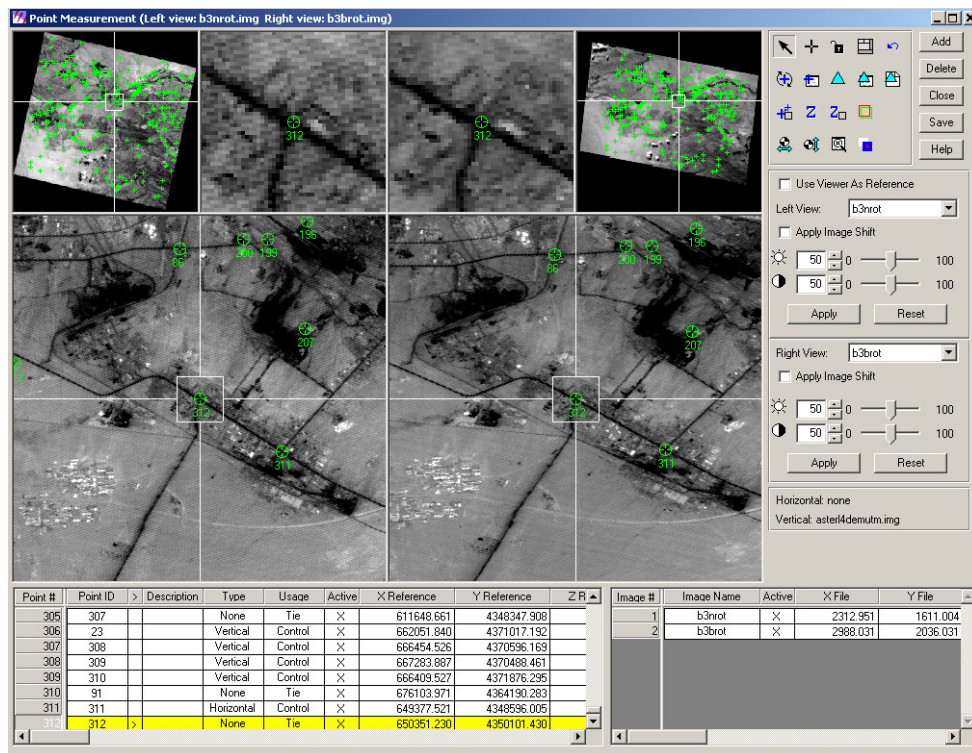
Fig 4.3: The distribution of tie points for exterior orientation

A relatively small amount of tie points were collected in this stage. The factors governing the overall performance of automatic tie point generation include (Erdas, 2001):
- Image quality (in this case the partial low correlation)
- Image content (in this case the Gobi, clouds)
- Topographic relief displacement (for example the mountainous area)
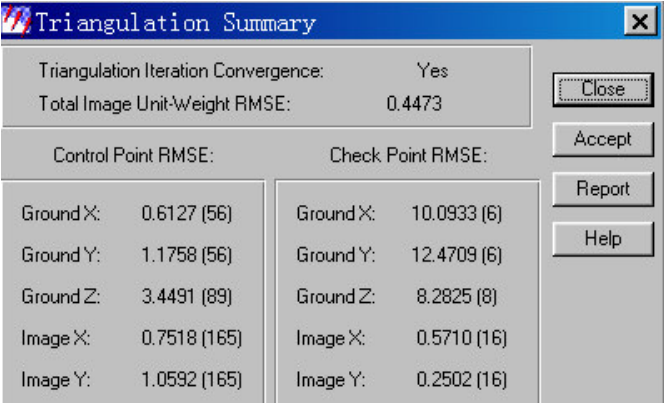
● Input quality of the minimum input requirement (for example the data accuracy)

Later on, using the *space forward intersection* technique, 3D-coordinates (i.e. mass points) were computed.

Careful experiments were performed during the triangulation stage. According to the triangulation report, some control points were excluded due to gross errors. At last, there were 39 "vertical", and 61 "full" GCPs accepted.

Furthermore, 8 check points were selected randomly from the Russian topographic map to test the triangulation results. They are distributed evenly, and including all terrain types. According to the status of the points, two check points were set to "vertical" as the exact x,y position could not be determined but only the z values.

The following triangulation result is obtained as shown in Figure 4.4. The triangulation report is presented in the Appendix.

Fig 4.4: Result of Triangulation

The number of observations for each field is shown in parentheses. The output image units: pixels; output ground units: meters; output angular units: radians.

Checking the mass points computed, there was a good relation with the elevations as derived from the topographic map. The southern Yellow River flood plain (alluvial fans) area had an average elevation range between 1100-1300 m; and the southwest mountainous region had an elevation range from 1600-2600m.

4.2.1 3D Modelling Process

The DEM can be generated and provided in several formats: DEM, TerraModel TIN, 3D Shape and ASCII. Before extraction, customed Advanced Properties can be set. For example, the cloud covering area can be excluded. So for each area a preferable strategy can be designed.

In this case, three strategies were used. For the mountainous area, and the rest relatively flat area, two user-defined strategies were applied showing improved performance. For the cloud and shadow parts, the default strategy named "exclude area" was directly used.

The outline of specific areas and associated strategies are shown below (Figure 4.5):
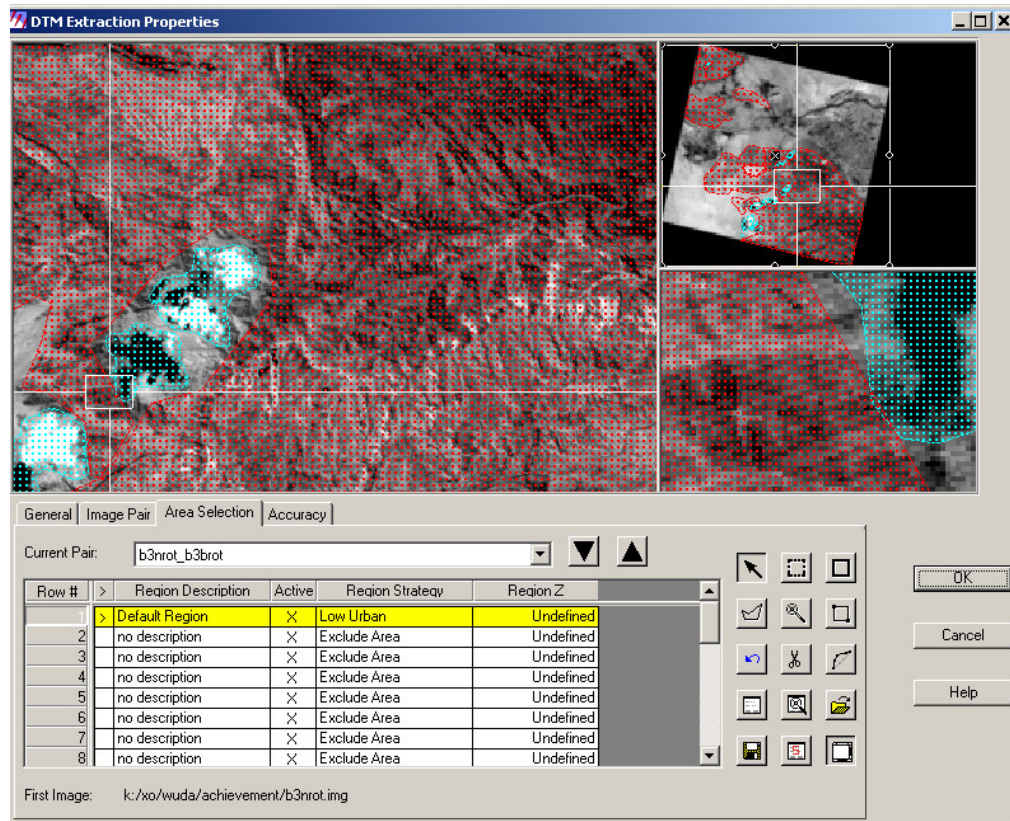
Fig 4.5: Area selection in DEM extraction with different strategies

High Mountains

Search Size = 5x3

Search Adaptive = TRUE

Correlation Size = 5x5

Correlation Adaptive = TRUE

Coefficient Limit = 0.8

Coefficient Adaptive = TRUE

Topographic Type = mountainous

Object Type = open_area

Use Band = 1

DEM Filtering = low

Low Urban

Search Size = 11x3

Search Adaptive = TRUE

Correlation Size = 7x7

Correlation Adaptive = TRUE

Coefficient Limit = 0.8

Coefficient Adaptive = TRUE

Topographic Type = rolling_hills
Object Type = low_urban
Use Band = 1
DEM Filtering = high

Exclude Area (defined by Erdas Imagine OrthoBase pro)
Search Size = 21x3
Search Adaptive = FALSE
Correlation Size = 7x7
Correlation Adaptive = FALSE
Coefficient Limit = 0.8
Coefficient Adaptive = FALSE
Topographic Type = rolling hills
Object Type = open_area
Use Band = 1
DEM Filtering = low

Where (Erdas, 2001):
Search Size is the search window size (in pixels) used to search for corresponding image points appearing within the overlap area of the left and right images. It is measured in the X and Y direction. Y direction is along the epipolar line; X direction is perpendicular to the epipolar line.
Correlation Size is the window size (in pixels) used for computing the correlation coefficient between image patches on the left and right images. It is measured in the X and Y direction.
Correlation Coefficient Limit is the minimum correlation value (i.e., threshold) for accepting a pair of points as matching candidates. The value ranges between 0 and 1, with 1 being the most accurate. Points that correlate below the coefficient limit are not considered in the DEM extraction. This figure can not be set lower than 0.5.

In this case, as for 1) High Mountains: the search size and correlation sizes are designed smaller as 5x3 and 5x5 respectively due to the relatively less mass points used for DEM interpolation, in order to improve the details of the resulting DEM. After comparing with several experiments, these parameters were decided. 2) Low Urban: this category was chosen because: first, the study area of Wuda coal fire field and the southern plains are around the cities; second, there are some rolling hills distributed within the borders of the image other than mountains. Identically after comparing with several experiments, these parameters were decided.
All of aforementioned user-defined parameters are set to "allow coefficient adaptive" for allowing for the changes with computing, in order to improve the results of the strategy application. Adaptive changes take place between iterative pyramid layer processing. Furthermore, the DEM Filtering parameter in the category of High Mountains is designed as "low" to keep the details in these areas, because less points were distributed here, the spikes can be edited during the post-processing stage (reference to section 4.3).
All the other parameters, including the category of Exclude Area, are set to default values as presented by Erdas IMAGINE OrthoBase pro.

For further processing, two output formats were selected for this research: 3D shape file and ASCII file. The former format is chosen for further processing in ESRI ArcView GIS and Erdas Stereo Analyst for 3D analyst and 3D modelling. It has three columns: Shape, Z, Status (based on correlation coefficient). The latter format is chosen for further processing in Erdas IMAGINE Dataprep module to interpolate 3D surface. It has five columns: the point ID, X, Y, Z, Status. By choosing the same DEM cell size for DEM computation in both formats, they are brought out the same number of mass points.

4.2.1.1 Grid-based Interpolation (Raster-DEM)

In a grid-based DEM an elevation is represented by the centre values of each pixel cell.

There can be two ways to generate grid format DEM (reference to section 3.3.3 of this thesis):

1) Reading ASCII file generated to create the 3D surface, A method "linear rubber sheeting", also called "spline" is used to calculate. This is a traditional geometric correction technique, based on performing geometric transformation to match control points, and the nearer, the more influence.

2) Generating into 3D Shape file to interpolate grid, using a method "IDW (Inverse Distance Weighted)", "Nearest Neighbours" algorithm.

The second interpolation method is preferable, because the mountainous areas which appear in the ASTER image are theoretically not appropriate to use the first method.

Those points with z values less than 900m and more than 3000m, which seemed with "wrong" elevations and having a correlation status > 1 (1=Excellent, 2=Good, 3=Fair, 4=Isolated, 5=Suspicious) have been removed. As a consequence, the remaining 31,620 mass points (with x, y and z coordinates) were used in further computation.

Some area on the image, for example the Gobi area is lack of data due to the low contrast on the original image pair, which reflects on the final DEM image as no data.

The extracted DEM in grid format is shown as (Figure 4.6):
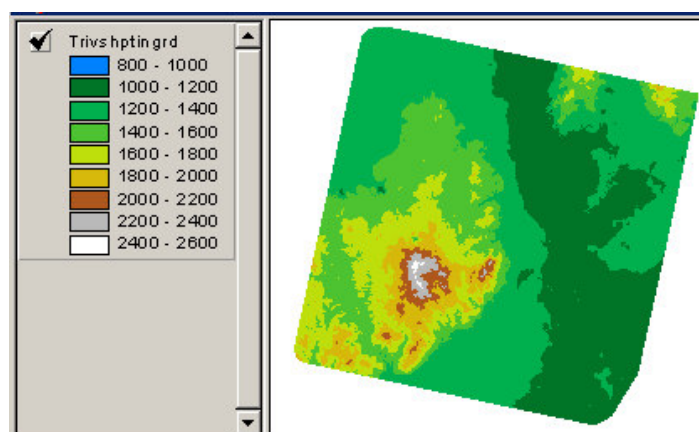
Fig 4.6: The grid-based DEM

4.2.1.2 TIN

In a TIN a system of irregular triangles represent the surface. It is possible to tag breaklines, whether hard or soft representing significant breaks in slope or insignificantly separating watersheds respectively, on the TIN to best represent the surface.

The 3D shape file generated during DEM Extraction was further processed to construct a TIN. In ArcVIEW, a TIN was computed as shown in Figure 4.7:
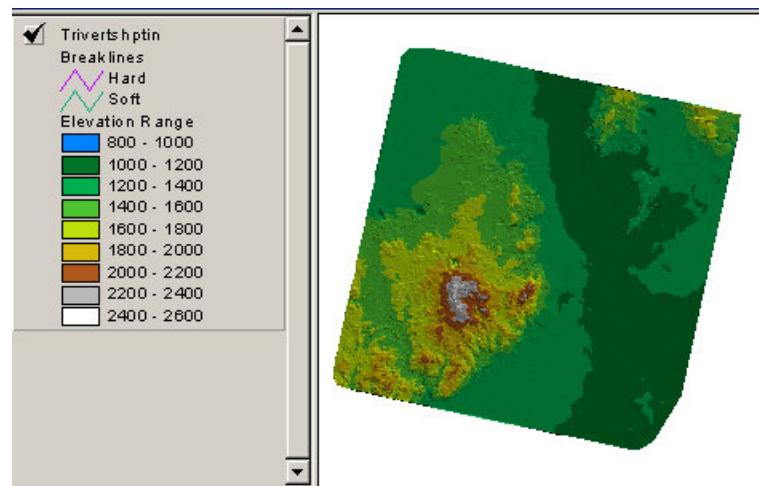
Fig 4.7: The TIN representative DEM

4.3   Modification

To increase the accuracy of the DEM extracted, the preliminary results have been modified in several ways:

- Adding more GCPs, simultaneously keeping them evenly distributed to ensure that the sensor is accurately modelled. Some points were added trying to distribute them in all kinds of terrain configurations, such as mountains and plains, and input points in some areas with few GCPs initial.

- Computing more tie points within the GCPs-defined coverage. 1) Carefully tested and designed the strategy parameters to increase the number of tie points (this step was performed resulting in the final parameters as are shown in Figure 4.2). 2) More GCPs also resulted in more tie points to be calculated. 3) Manually adding more tie points on the image pair by visual observations. The relatively larger amount of tie and GCPs allows for the minimization and distribution of errors throughout the whole data block.

- Modifying the gross error points that were obtained during the triangulation. According to the triangulation report, bad points were found and checked. Those points that were excluded with gross errors have been re-positioned on the image pair. All the tie points and GCPs have been adjusted to correlate till pixel-level in order to ensure the precision of pointing as high as possible, since the points for computation are relatively less. This process was carried out during the exterior orientation (as mentioned in section 4.2), simultaneously verifying the quality of the control points.

- Filling local depressions (sinks). A script named "Spatial DEMFill" provided by ESRI (www.esri.com) was used to modify those sinks. The content of this Avenue script is presented in the Appendix.
- DEM editing. There are two options for editing the DEM: editing the DEM image by recalculating the anomalies (smoothing the spikes and pits in the data) through Erdas IMAGINE "Raster interpolation" function; editing the 3D shape file in Stereo Analyst focusing on the x, y, z coordinates.

4.4   Final Outcome

For a better presentation of the terrain characteristics, the final outcome of the DEM extraction process in this study is presented in two formats: Raster-DEM (Figure 4.8) and TIN (Figure 4.9).
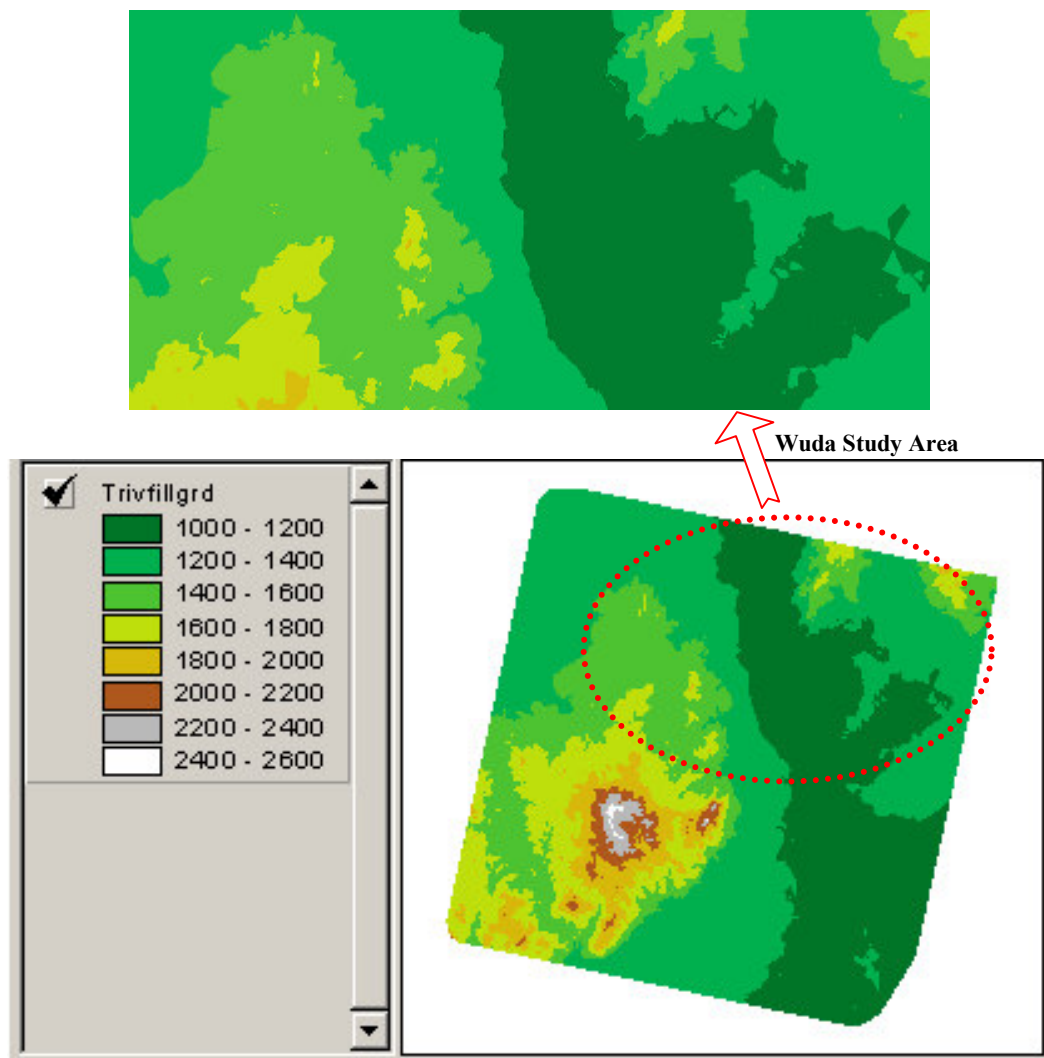
Fig 4.8: The final raster-DEM output
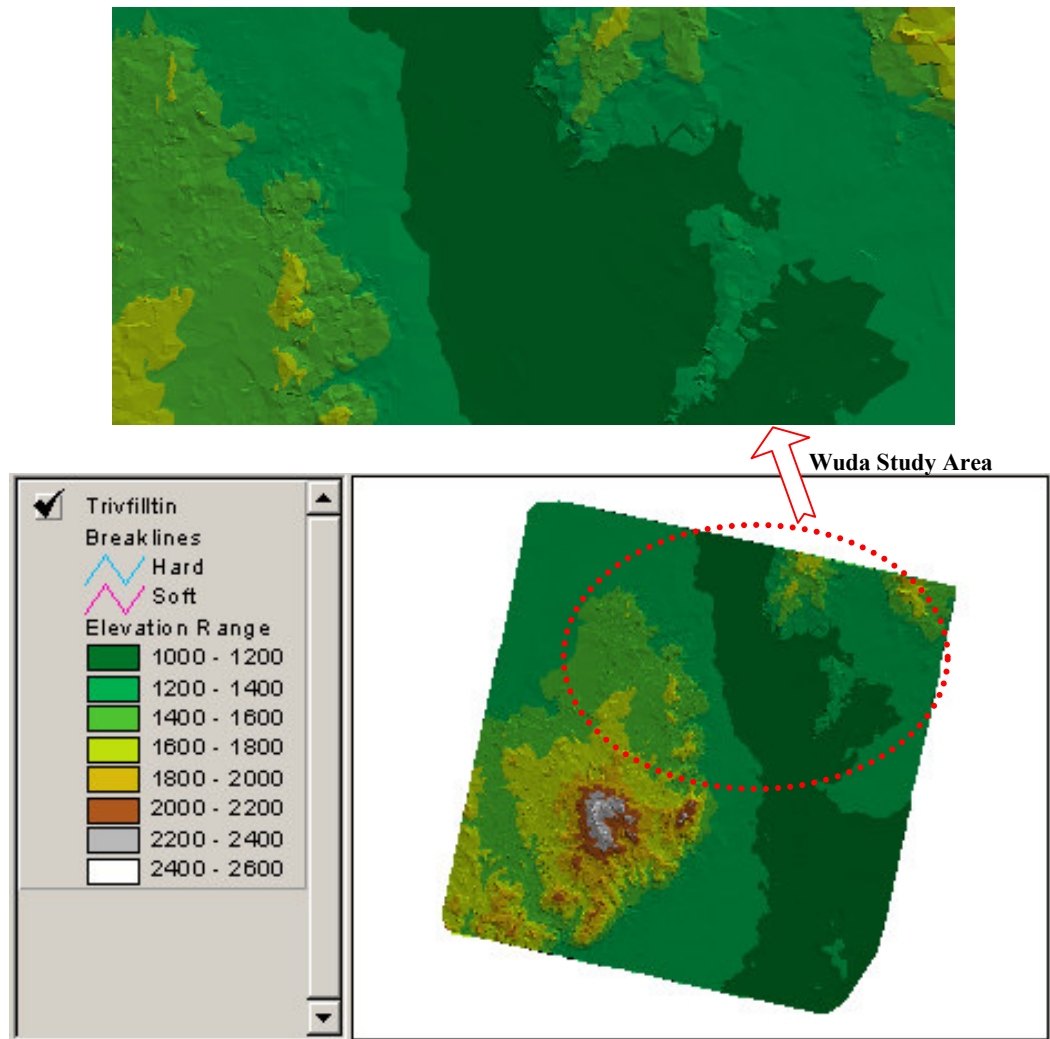
Fig 4.9: The final DEM output in TIN form

4.5   Orthorectification

Orthorectification is the process of reducing geometric errors inherent within photography and imagery. The variables contributing to geometric errors include, but are not limited to:

• sensor orientation

• systematic error associated with the sensor

• topographic relief displacement

• Earth curvature

The orthorectification process removes the geometric distortion of the sensors, topographic relief displacement, and systematic errors associated with the imagery. An orthorectified image is a planimetrically true image with exact x and y ground –truth coordinates. A GIS (Geographic Information System) accepts an ortho image as the ideal reference of the ground location for the creation and maintenance of vector data. We can say that an orthoimage has the geometric characteristics of a map and the image qualities of a photograph. Any measurement taken on an orthoimage reflects a measurement taken on the ground.

After qualified exterior orientation, an ortho-image can be generated. In this case, the ASTER 3N image was used to create the ortho-image, because this nadir recorded image has less terrain relief displacement compared to the backward looking image.

The ortho-image is shown below (Figure 4.10):

690716.00, 4342692.71   (UTM / WGS 84)
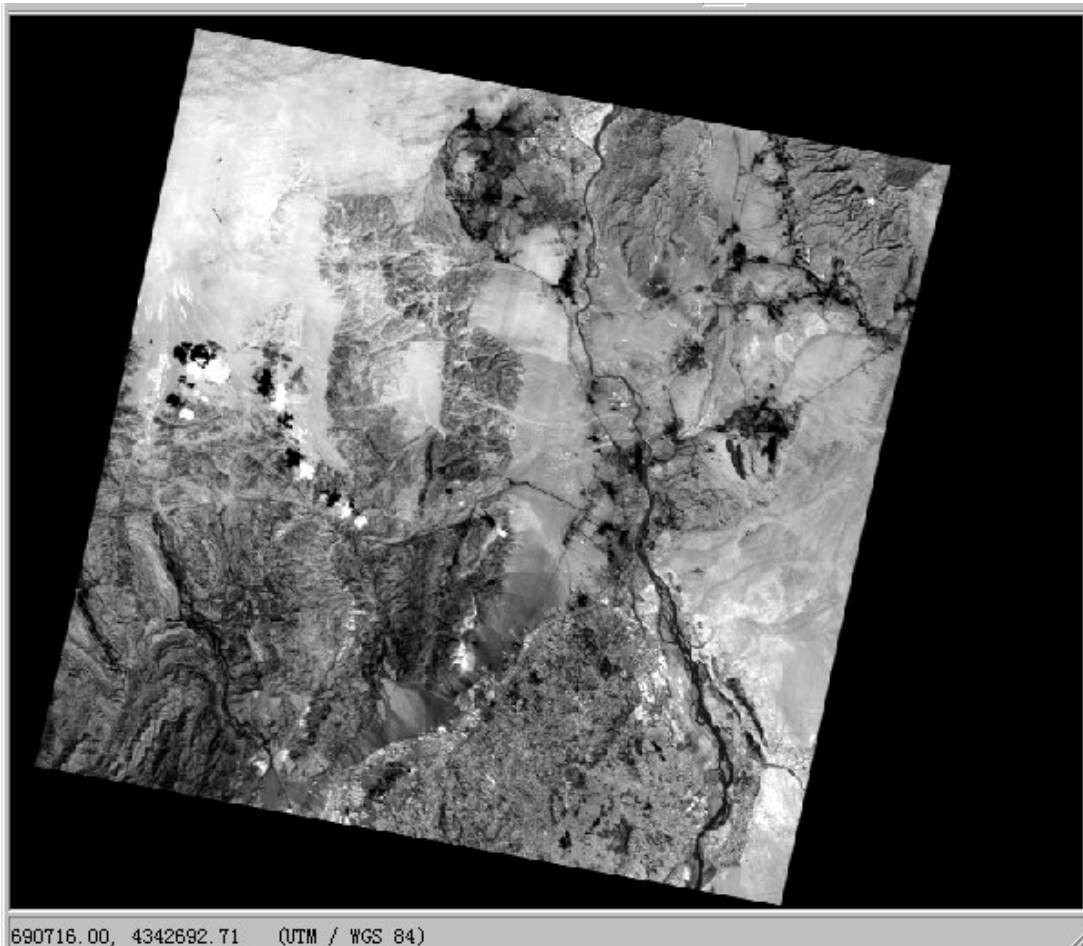
Fig 4.10: The ortho-image created for the Wuda Coal Fire research project

5. Accuracy Assessment and Discussion

Scope of the Accuracy Assessment The given topographic map served as a main data source in this study for DEM extraction. Figure 5.1 shows the extent of the map in comparison to the ASTER image.
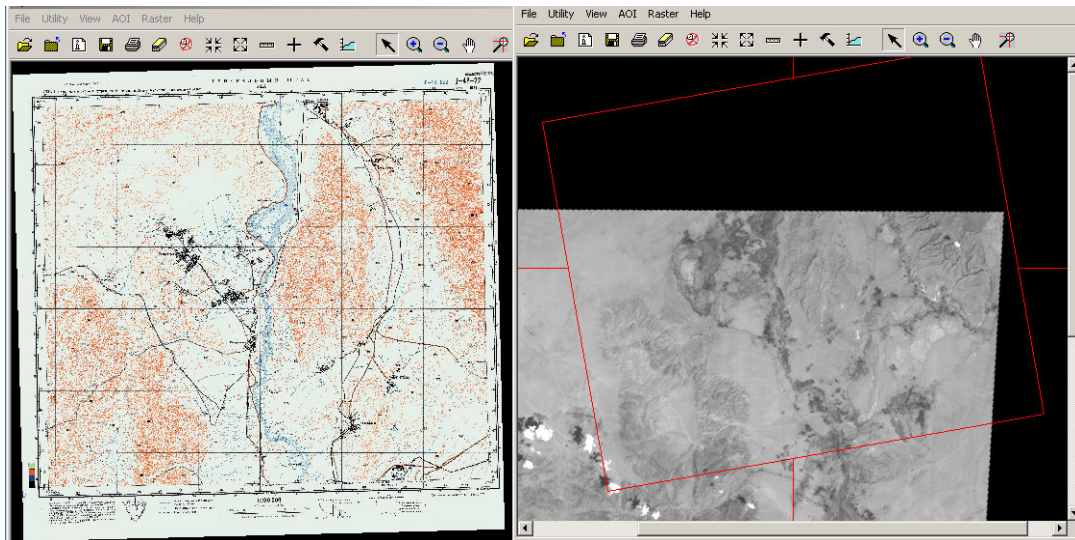
Fig 5.1: The extent of the topographic map corresponding to the image

The accuracy of the final DEM is limited by the following factors:

- Available data. Due to lack of 1:50,000 scale topographic map, which normally matches the requested accuracy in height reading, there was only a 1:100,000 scale topographic map of 1978. The elevation accuracy that can be obtained from such a map is limited. In addition, the quality of the remote sensing imagery, such as the clouds and shadows and some parts of low-correlation in this case, will influence the ultimate accuracy.
- Measurement equipment. The GPS receiver used in the fieldwork has a medium accuracy of ±10m in planimetry, but a low accuracy (up to 50m) in altimetry. Therefore a limited number of points could be selected and no creditable GPS height data could be used.
- Data processing. Other errors associated with regard to the procedure of DEM extraction affecting the data accuracy:
    1) Systematic errors. This kind of errors usually can be judged by certain rules, for example, the inaccuracy follows a common direction or magnitude.
    2) Blunders. This kind of errors is usually due to mis-measuring, wrongly input, poor quality of data sources, and other man-made mistakes.
       In practice, the measurement of common points on both images is very important. The precision of position has a major influence on the output accuracy. However, we

should not change the positions of points just comparing the triangulation report. The actual situation, for instance the corresponding positions on images, needs to be regarded, because a) the accuracy statistics reflect the conforming status of each point to the whole constructed triangulation, but not directly reflect the ground-truthing accuracy; b) every point would be affected after every modification, the previous better ones probably become worse; c) the better points in triangulation could be the worse ones in the DEM generated afterwards. Therefore, careful experiments are necessary in order to find the most appropriate number of "full" points, and find out the best way to modify the points, i.e. transfer the type to "vertical" or check the positions of the points on both images.

3) Random. This kind of errors is difficult to predict, having incident and unknown causes. Normal random errors are subject to statistical normal distribution.

Usually, in the border areas mass points having lower accuracy are obtained; flat areas have higher accuracy than mountainous areas in reading z coordinates from map.

When selecting extra control points, a fact was that in the mountainous area it is very difficult to obtain coordinates; due to the changing relief in this kind of terrain, there should be more control points measured here. That is to say, the spatial resolution in mountains needs to be higher than flat areas to reflect the "real world". In point measuring, some clearer intersections existing in mountainous area were selected. The higher the resolutions are, the easier and more precise positions can be determined in this area.

5.1   General Assessment

This assessment method to get a general accuracy impression of the results obtained is by comparison of the output and the original data.

All the general assessment methods are performed by checking the conformance focusing on apparent features, such as the mountains, the Yellow River, and the drainage directions.

The two data items, saying the checking and the checked ones, will be observed and compared from the beginning until the end of the features. The positions, the distribution scopes, and the terrain tendency will be researched carefully.

5.1.1 Compare the Terrain Relief and the Features

In Virtual GIS, exaggerating the elevation of the DEM in a 3D virtual viewing, checking for example the Yellow River and other clear features by linking it with the ortho-image, a general visual impression can be obtained showing that the general terrain relief is correctly represented (Figure 5.2):
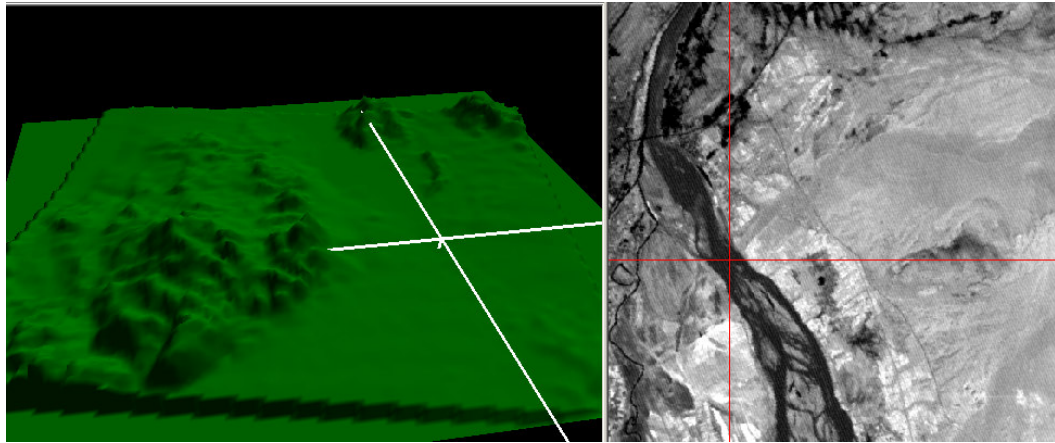
Fig 5.2: The conformance between DEM and Ortho-image

5.1.2 Compare the Features of DEM and the Original Topographic Map

In Erdas IMAGINE Viewer, the DEM generated and the Russian topographic map can be linked, using the swiping function the conformance of the features between both can be visually assessed. In general the results obtained are acceptable, as Figure 5.3 shows:
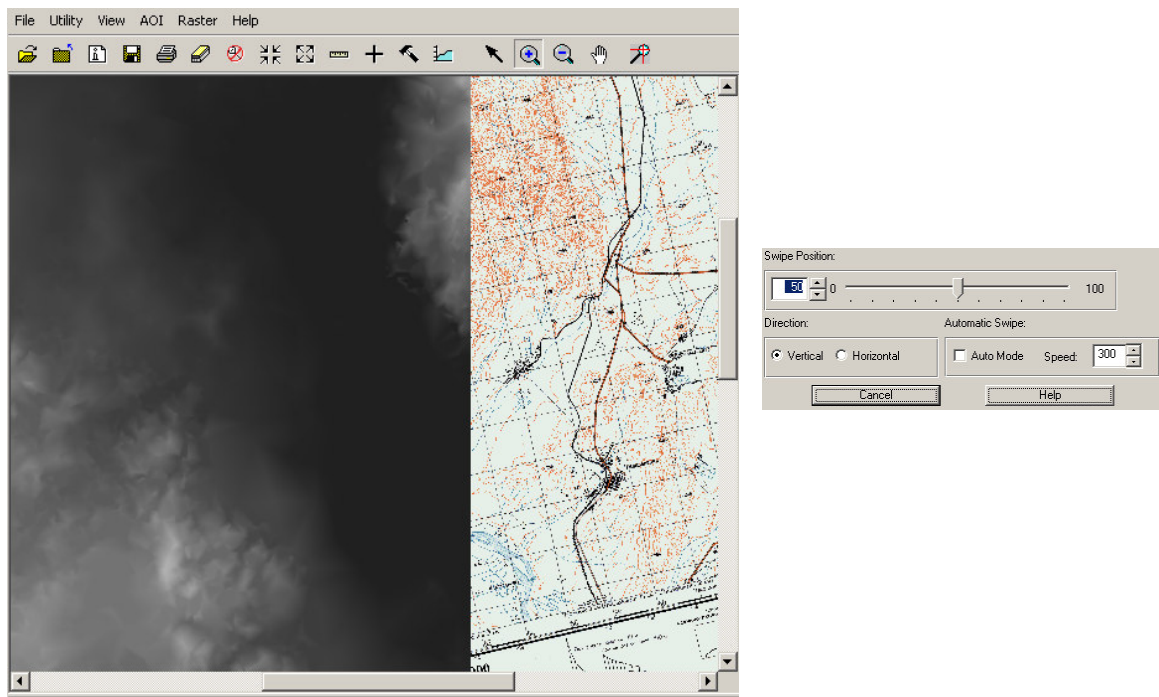
Fig 5.3: Swipe DEM on the original topographic map to check the conformance

5.1.3 Overlay the Generated Contour Map on the Russian Top Map

The contour map generated after DEM extraction for this study is used, having a 20m interval. The contour lines are overlaid on the original Russian topographic map. As Figure 5.4 shows, visually the two maps have a good conformance in the common area. The terrain characteristics in mountainous area, and the directions of drainages correspond to the contour lines generated.
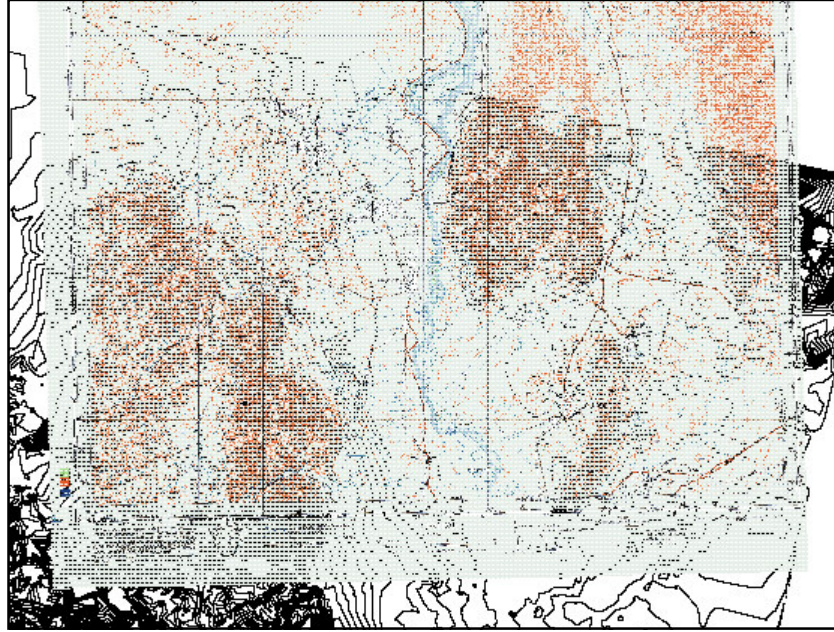
Fig 5.4: The conformance between the DEM-generated contour map and the original map

5.2 Compare with Check Points

Check Points can be defined from GCPs, tie points and user-defined points. In this case, 46 user-defined points were freely chosen within the border of the topographic map used as ground-truth data in this study as check points.

An algorithm of accuracy evaluation named Root Mean Square Error (RMSE) was used in this method. It encompasses both systematic and random errors, and is defined as:

$$m_z = \sqrt{\frac{1}{n}\sum_{i=1}^{n} \delta Z_i^{\,2}} \qquad (1)$$

Where m_z = RMSE of elevation

δZ_i = Elevation differences between the derived DEM and the check points

N = Number of check points

The accuracy assessment result is presented by OrhtoBASE Pro's DTM Extraction Report, which is shown in the Appendix. The detailed point accuracy information is shown in Table 5.1.

The total statistic results (unit in meters) are shown below.

> Block GCP to DEM Vertical Accuracy
> Total # of GCPs Used: 46
> Minimum, Maximum Error: -50.3625, 61.2698
> Mean Error: 7.8272
> Mean Absolute Error: 23.4312
> **Root Mean Square Error: 28.1646**

Where (reference to Erdas OthoBase pro document):

Minimum, Maximum Error: This field lists the minimum residual and maximum residual values of all 3D reference information.

Mean Error: This field lists the mean residual error for all 3D reference information. Mean is calculated by adding the error of all the points, then dividing by the total number of points.

Mean Absolute Error: This field is the mean of all negative errors. This item implies how much the accuracy result deviates from a systematic error. It could be assumed that if this value is 0, meaning that all of the residuals are plus values, mostly like a systematic error.

Root Mean Square Error (RMSE): RMSE is a global indicator of the quality of the output DEM (reference to formula (1)). The lower the RMSE, the better the solution.

From the statistical results it is clear that:
1) the differences of elevations between the computed values and the input values are mostly less than 50 meters (see Table 5.1);
2) the mean error is less than 8 meters, saying that the major differences are several meters, the bigger errors are minor;
3) the mean absolute error is around 23 meters, not very big, meaning that the distribution of the errors is within the normal extent;
4) the total RMSE is lower than 30 meters, close to the reading error range of the topographic map used for the DEM extraction in this study;

Therefore, the DEM acquired can be regarded as acceptable.

Pt.ID	X	Y	Z	DTM Z	Residual
1	648183.0595	4370941.0041	1120.0000	1150.6379	30.6379
2	647343.3849	4373354.3344	1126.0000	1142.6285	16.6285
3	646494.9026	4373028.4467	1132.0000	1169.9118	37.9118
4	662396.2641	4365432.5859	1210.0000	1185.2775	-24.7225
5	661171.5780	4368818.6140	1170.0000	1173.2216	3.2216
6	664588.0159	4356871.3421	1189.0000	1177.1506	-11.8494
7	636975.9335	4366614.5663	1320.0000	1350.1483	30.1483
8	648127.0641	4365459.3048	1126.0000	1138.4129	12.4129
9	646968.6650	4366333.9881	1138.0000	1160.8318	22.8318
10	646002.6174	4366287.5854	1149.0000	1172.0834	23.0834
11	670280.3673	4366010.8398	1250.0000	1217.1519	-32.8481
12	669342.2702	4367215.3154	1240.0000	1258.6892	18.6892
13	665625.3893	4368794.8430	1208.0000	1225.6857	17.6857
14	649195.3983	4375780.0926	1104.0000	1117.0293	13.0293
15	649295.7750	4374487.6014	1108.0000	1116.9643	8.9643
16	650064.9873	4373644.9909	1099.0000	1098.4181	-0.5819
17	648861.1965	4364332.2372	1118.0000	1107.5853	-10.4147
18	658872.7062	4361314.1064	1159.0000	1150.1516	-8.8484
19	663367.2254	4356849.3931	1178.0000	1164.3266	-13.6734
20	663872.6421	4355727.0413	1190.0000	1186.2252	-3.7748
21	667376.6352	4356597.0604	1202.0000	1187.3608	-14.6392
22	662212.8275	4360569.1203	1218.0000	1219.1698	1.1698
23	659828.8627	4368656.3795	1170.0000	1231.2698	61.2698
24	640521.7049	4371961.6632	1260.0000	1311.2857	51.2857
25	643832.7527	4378329.9931	1120.0000	1168.9091	48.9091
26	644425.8096	4376022.3561	1139.0000	1178.3208	39.3208
27	646169.7490	4373432.8704	1130.0000	1176.6245	46.6245
28	632806.3360	4363299.3507	1438.0000	1473.8761	35.8761
29	634232.2783	4364766.0201	1400.0000	1453.2402	53.2402
30	650702.8170	4360591.1349	1105.0000	1132.0950	27.0950
31	623967.5374	4327072.5061	1320.9910	1351.9690	30.9780
32	627656.5566	4337976.7794	1881.9150	1919.9514	38.0364
33	634513.7561	4333764.4418	1464.2900	1434.1445	-30.1455
34	637483.9108	4355422.0645	1501.5190	1498.2132	-3.3058
35	648130.9717	4354481.6523	1220.0790	1204.2990	-15.7800
36	649694.0259	4358814.3494	1177.2430	1148.5852	-28.6578
37	644125.4254	4350503.0755	1332.0220	1344.8552	12.8332
38	620710.0996	4349288.2787	1684.6290	1634.2665	-50.3625
39	618465.7742	4345733.0046	1624.6020	1637.0881	12.4861
40	653299.7210	4348699.6416	1150.7030	1170.7117	20.0087
41	651900.8286	4378718.9594	1152.7210	1141.1262	-11.5948
42	655767.5036	4374869.5508	1660.7540	1632.6253	-28.1287
43	652038.0209	4354656.3673	1167.6130	1164.3975	-3.2155
44	652953.8088	4351894.9325	1154.2590	1158.8253	4.5663
45	668211.4692	4368551.4853	1292.2850	1249.1430	-43.1420
46	667584.1368	4373591.2504	1320.4470	1297.2399	-23.2071

Table 5.1: The result of Accuracy Assessment of the DEM extracted by Check points

Concentrate on the topographic map extent

In order to obtain an idea of the accuracy of the study area, this area (as Figure 5.5 shows) was analysed into more detail.
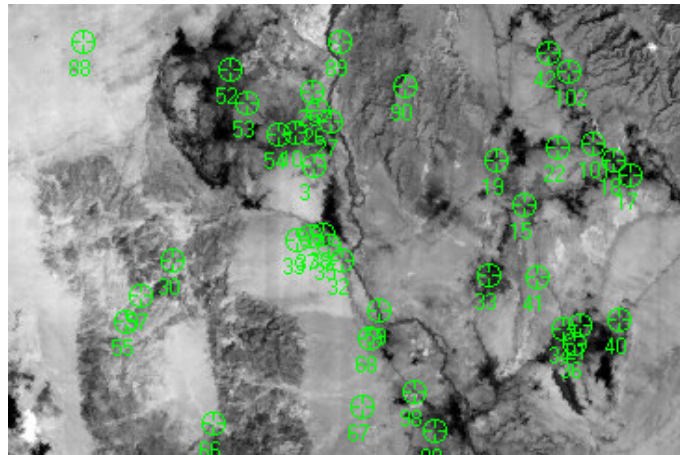
Fig 5.5: The distribution of the well-defined GCPs
within the topographic map extent for accuracy assessment

According to different geomorphologic units in this area, some GCPs are used as check points for the accuracy assessment. The results of the accuracy assessment associated with geomorphologic terrain types are shown from Table 5.2 to Table 5.8:

Table 5.2: Assessment for Wuda Syncline area

	Point ID	Z	DEM Z	Residual
Wuda Syncline, Around the City	3	1120	1151	31
	10	1126	1143	17
	12	1132	1170	38
	25	1104	1117	13
	26	1108	1117	9
	52	1120	1169	49
	53	1139	1178	39
	54	1130	1177	47
	RMSE = 33.6805			
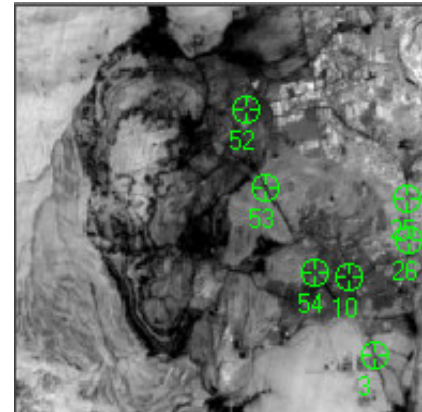
Table 5.3: Assessment for middle alluvial fans

	Point ID	Z	DEM Z	Residual
Middle Alluvial Fans	32	1118	1108	-10
	35	1126	1138	12
	37	1138	1161	23
	38	1130	1141	11
	39	1149	1172	23
	68	1177	1149	-28
	98	1168	1164	-4
	RMSE = 17.8205			
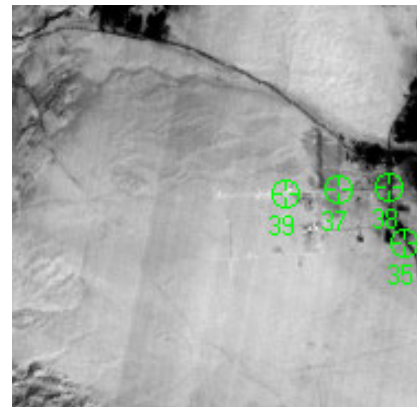
Table 5.4: Assessment for lower fans

	Point ID	Z	DEM Z	Residual
Lower Fans Along the Yellow River	27	1099	1098	-1
	59	1105	1132	27
	89	1153	1141	-12
	99	1154	1159	5
	RMSE = 14.9917			
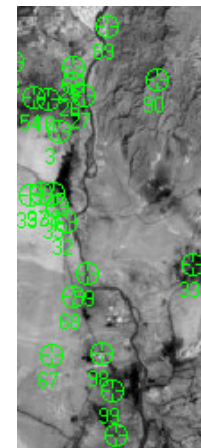
Table 5.5: Assessment for high mountains

	Point ID	Z	DEM Z	Residual
High Mountains	90	1661	1642	-19
	check1	1515	1469	-46
	check2	1520	1605	85
	RMSE = 56.8683			
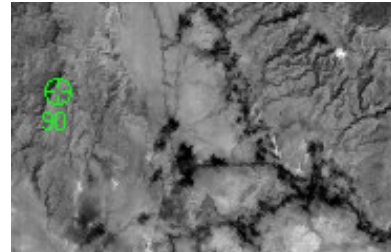
Table 5.6: Assessment for middle mountains

	Point ID	Z	DEM Z	Residual
Middle Mountains	30	1320	1346	26
	55	1438	1463	25
	57	1400	1449	49
	66	1502	1485	-17
	RMSE = 31.5872			
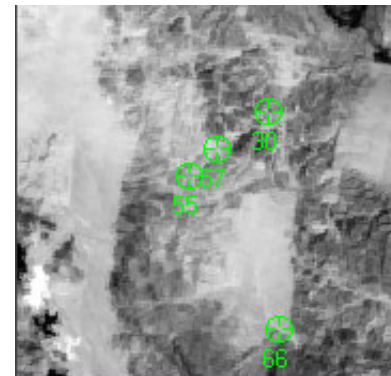
Table 5.7: Assessment for Gobi area

	Point ID	Z	DEM Z	Residual
Gobi Area	88	1324	1287	-37
	check3	1258	1316	58
	check4	1240	1309	69
	RMSE = 56.2554			
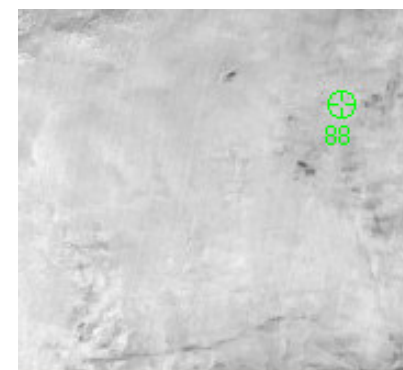
Table 5.8: Assessment for other area within the extent of the topographic map

	Point ID	Z	DEM Z	Residual
Other Area	15	1210	1188	-22
	19	1170	1173	-3
	21	1189	1177	-12
	22	1208	1226	18
	33	1159	1150	-9
	34	1178	1164	-14
	36	1190	1186	-4
	40	1202	1187	-15
	41	1218	1221	3
	17	1250	1217	-33
	18	1240	1258	18
	42	1170	1218	48
	101	1292	1251	-41
	102	1320	1300	-20
RMSE = 22.8129				
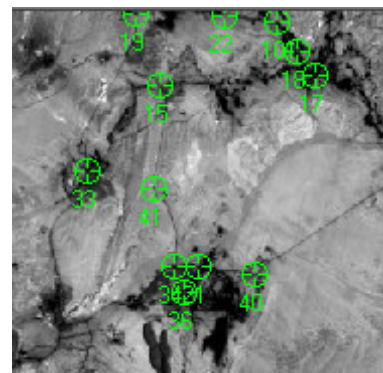
Total RMSE for the selected areas in comparison with the topographic map = 31.5012

The statistical results given by this accuracy assessment are acceptable.

Other than High mountains and Gobi area, all the terrain types are represented by the DEM heights within the normal range of accuracy.

A general trend can be observed: the lower the terrain is, the smaller the error is. Due to normally the higher accuracy in flat area than the mountainous area, the precision of point measurement affects the ultimate accuracy of the extracted DEM.

The Gobi area and the high mountainous area suffer from a lack of data due to the difficulty of exact positioning during selecting of Ground Control Points from the topographic map. Therefore it is impossible to choose clear features in these areas as check points. For giving most detailed accuracy information about the DEM extracted in this case, user-defined spot height data (extra 2 points respectively), read from the topographic map and corresponding DEM common points, are input as the check points for vertical accuracy assessment. The RMSEs in these types are higher than the others in the order of GCP plotting accuracy.

5.3   Compare with ASTER L4 DEM

The ASTER L4 DEM is provided by ASTER Science Team. This DEM is obtained without ground-truth evaluation. 46 check points (as given in Table 5.1) are used to check the accuracy of the DEM extracted to compare the differences of elevations between ASTER L4 DEM and ground-truth data on these common positions. The results are shown in Table 5.9.

The overall RMSE is 65.4582. Comparing to the result of the accuracy assessment of the DEM extracted for this study, which is 28.1646, this error is larger. The conclusion of this assessment method can be: the DEM extracted is closer to the ground-truth data used in this study, as compared to the ASTER L4 DEM that is created without ground-truthing.

Points No.	X	Y	Z	ASTER L4 DEM Z (Zast)	Residual
1	648183.0595	4370941.0041	1120.0000	1199.345	79.345
2	647343.3849	4373354.3344	1126.0000	1218.110	92.11
3	646494.9026	4373028.4467	1132.0000	1222.031	90.031
4	662396.2641	4365432.5859	1210.0000	1227.042	17.042
5	661171.5780	4368818.6140	1170.0000	1232.329	62.329
6	664588.0159	4356871.3421	1189.0000	1196.163	7.163
7	636975.9335	4366614.5663	1320.0000	1438.245	118.245
8	648127.0641	4365459.3048	1126.0000	1192.905	66.905
9	646968.6650	4366333.9881	1138.0000	1225.971	87.971
10	646002.6174	4366287.5854	1149.0000	1242.291	93.291
11	670280.3673	4366010.8398	1250.0000	1270.881	20.881
12	669342.2702	4367215.3154	1240.0000	1306.505	66.505
13	665625.3893	4368794.8430	1208.0000	1266.005	58.005
14	649195.3983	4375780.0926	1104.0000	1155.712	51.712
15	649295.7750	4374487.6014	1108.0000	1167.459	59.459
16	650064.9873	4373644.9909	1099.0000	1164.029	65.029
17	648861.1965	4364332.2372	1118.0000	1168.100	50.1
18	658872.7062	4361314.1064	1159.0000	1191.896	32.896
19	663367.2254	4356849.3931	1178.0000	1188.396	10.396
20	663872.6421	4355727.0413	1190.0000	1187.450	-2.55
21	667376.6352	4356597.0604	1202.0000	1209.662	7.662
22	662212.8275	4360569.1203	1218.0000	1278.718	60.718
23	659828.8627	4368656.3795	1170.0000	1225.393	55.393
24	640521.7049	4371961.6632	1260.0000	1387.670	127.67
25	643832.7527	4378329.9931	1120.0000	1195.395	75.395
26	644425.8096	4376022.3561	1139.0000	1223.108	84.108
27	646169.7490	4373432.8704	1130.0000	1218.748	88.748
28	632806.3360	4363299.3507	1438.0000	1573.653	135.653
29	634232.2783	4364766.0201	1400.0000	1508.739	108.739
30	650702.8170	4360591.1349	1105.0000	1126.792	21.792
31	623967.5374	4327072.5061	1320.9910	1267.294	-53.697
32	627656.5566	4337976.7794	1881.9150	1915.106	33.191
33	634513.7561	4333764.4418	1464.2900	1295.820	-168.47
34	637483.9108	4355422.0645	1501.5190	1509.350	7.831
35	648130.9717	4354481.6523	1220.0790	1221.085	1.006
36	649694.0259	4358814.3494	1177.2430	1183.917	6.674
37	644125.4254	4350503.0755	1332.0220	1328.946	-3.076
38	620710.0996	4349288.2787	1684.6290	1693.808	9.179
39	618465.7742	4345733.0046	1624.6020	1681.540	56.938
40	653299.7210	4348699.6416	1150.7030	1146.279	-4.424
41	651900.8286	4378718.9594	1152.7210	1146.392	-6.329
42	655767.5036	4374869.5508	1660.7540	1709.337	48.583
43	652038.0209	4354656.3673	1167.6130	1166.305	-1.308
44	652953.8088	4351894.9325	1154.2590	1160.290	6.031
45	668211.4692	4368551.4853	1292.2850	1291.558	-0.727
46	667584.1368	4373591.2504	1320.4470	1319.177	-1.27
RMSE = SQRT((SUMSQ(Zast – Z))/46) = 65.4582					

Table 5.9: The ground-truth evaluation of the ASTER L4 DEM

5.4   Other Assessment Methods

For accuracy assessment, besides the above-mentioned methods, it is possible to use other methods to evaluate the achievement, including:

- Profiling or measuring on other standard DEMs, for example the DEM generated from contour map(s), or from other high-resolution satellite image pair(s), to compare the common spots;
- Acquiring spot height data from latest topographic map to be as check points;
- Taking field data from highly precise Differential GPS to assess the results;
- Verifying the conformance of the features and the DEM-representing terrain characteristics by overlaying other ground control outcomes on the DEM extracted in this case

Different options of assessment give different results. However, the resulting accuracy should be around the input data precision range. Based on varied data acquiring conditions, appropriate methods can be applied to the evaluation.

For DEM extraction from the ASTER image pair that is with relatively weak topographic data sources, the statistical results of the accuracy assessment of the DEM extracted for this research show that the results are acceptable. The accuracy obtained is around the precision range of the source data (topographic map).

6. Output and Derived Product

Foreseen uses of ASTER DEM include the creation of perspective views for day-time thermal image correction (using slope and aspect elements) and other earth science study. For example, coal fire researchers will probably drape the ASTER multispectral VNIR, SWIR, and TIR images over the DEM covering the corresponding area.

6.1 Virtual GIS

In the Virtual GIS module of Erdas Imagine, a 3D scene was created to perform roaming within a virtual 3D environment. Requested features can be viewed and queried.

For this coal fire research, a false-color ASTER image of Band 1-2-3 was overlaid on the DEM extracted in this study for a "real-world" view. A sample is shown in Figure 6.1:
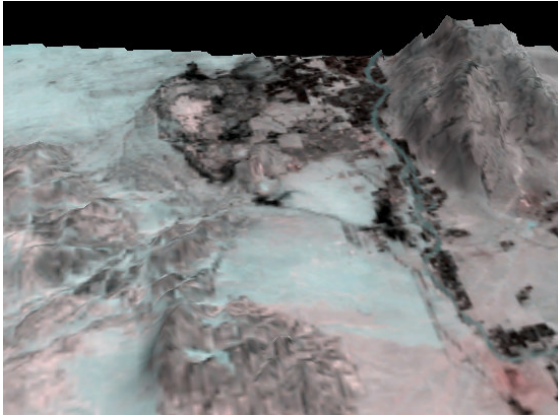
A 3D View of
Wuda Coal Field
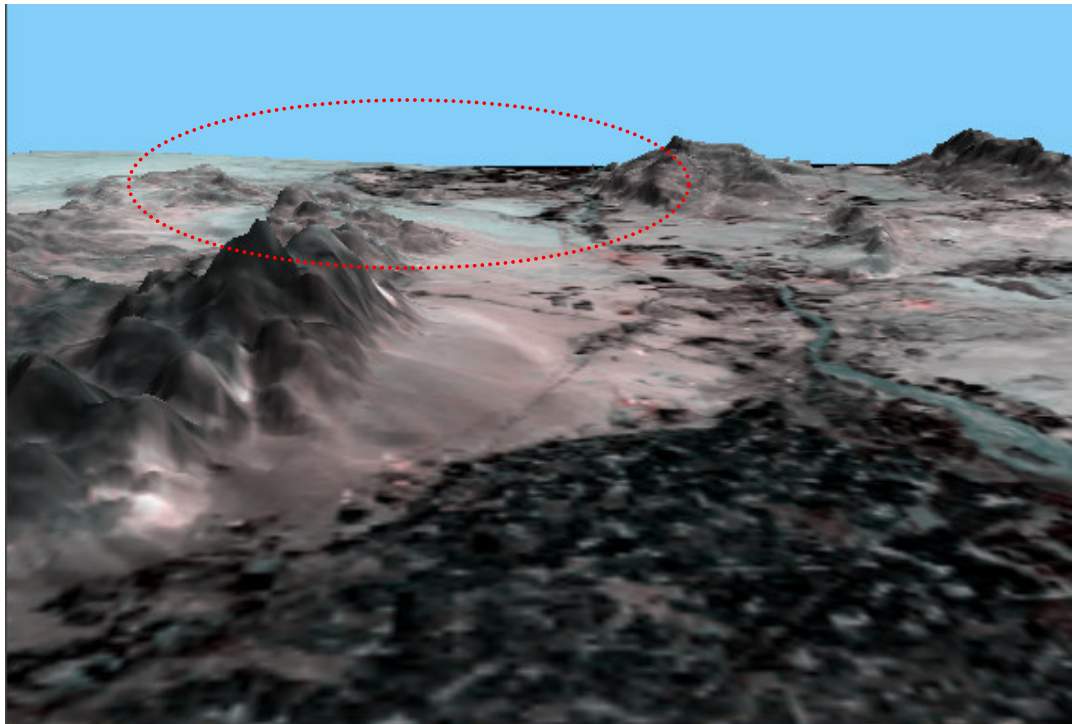
Fig 6.1: Virtual world presentation of the DEM

6.2   Slope and Aspect output

The DEM generated in this study can allow operations on the 3D surfaces: the applier can determine the elevation at any point of the model. Moreover, a DEM can be used to calculate the slope steepness and aspect serving for terrain analysis.

A surface has steepness and direction, commonly referred to as slope and aspect.

Slope is expressed as the change in elevation over the distance of each pixel size, identifying the inclination of a surface. It is most often expressed as a percentage, but can also be calculated in degrees. The relationship between percentage and degree expression of slope (Erdas, 2001) is as follows:

- A 45° angle is considered a 100% slope

- A 90° angle is considered a 200% slope, hence:

- Slopes less than 45° fall within the 1-100% range

- Slopes between 45° and 90° are expressed as 100-200% slopes

A 3 x 3 pixel window is used to calculate the slope at each pixel. For a pixel at location X,Y, the elevations around it are used to calculate the slope as shown in Figure 6.2:

a,b,c,d,f,g,h, and i are the elevations of the pixels around it in a 3 X 3 window.
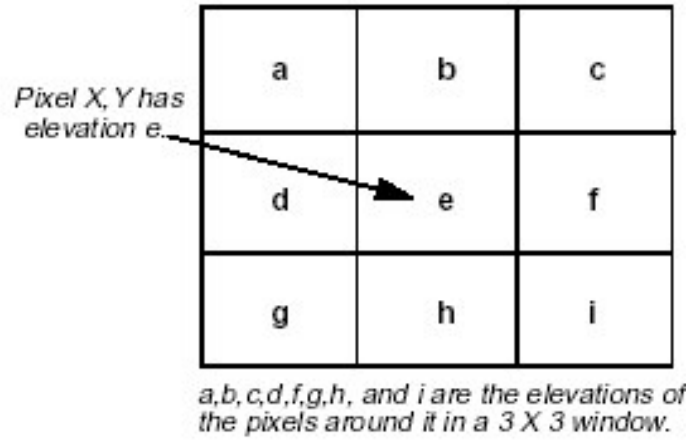
Fig 6.2: 3x3 Window used to calculate the slope at each pixel

The average elevation changes per unit of distance in the x and y direction (Δx and Δy) are calculated as:

$$\Delta x_1 = c - a \qquad\qquad \Delta y_1 = a - g$$
$$\Delta x_2 = f - d \qquad\qquad \Delta y_2 = b - h$$
$$\Delta x_3 = i - g \qquad\qquad \Delta y_3 = c - i$$

$$\Delta x = (\Delta x_1 + \Delta x_2 + \Delta x_3)/3 \times x_s$$

$$\Delta y = (\Delta y_1 + \Delta y_2 + \Delta y_3)/3 \times y_s$$

Where the x_s *and* y_s are the x,y pixel size respectively.
The slope at pixel x,y is calculated as:

$$s = \frac{\sqrt{(\Delta x)^2 + (\Delta y)^2}}{2}$$

$$if \ s \leq 1 \qquad percent \ slope \ = \ s \times 100$$

$$if \ s > 1 \qquad percent \ slope \ = \ 200 - \frac{100}{s}$$

$$slope \ in \ degrees \ = \ \tan^{-1}(s) \times \frac{180}{\pi}$$

Aspect is the direction the surface faces at each pixel. It is expressed in degrees from north, clockwise, from 0 to 360. Due north is 0 degrees. A value of 90 degrees is due east, 180 degrees is due south, and 270 degrees is due west. A value of -1 degrees is used to identify flat surfaces such as water bodies.

Similar to the slope calculation, a 3x3 window is used to calculate the aspect of a pixel from the average changes of elevation in x and y directions. While the Δx and Δy are calculated as:

$$\Delta x \ = \ (\Delta x_1 + \Delta x_2 + \Delta x_3)/3$$

$$\Delta y \ = \ (\Delta y_1 + \Delta y_2 + \Delta y_3)/3$$

If $\Delta x = 0$ and $\Delta y = 0$, then the aspect is flat (coded to 361 degrees). Otherwise, θ is calculated as:

$$\theta \ = \ \tan^{-1}\left(\frac{\Delta x}{\Delta y}\right)$$

Then aspect is $180 + \theta$ (in degrees).

Slope and aspect images are often an important factor in assessing the suitability of a site for a proposed use (Erdas, 2001):

• Slope can be used to calculate the shortest and most navigable path over a mountain range for constructing a road or routing a transmission line，

• Aspect influences the growth of vegetation due to the availability of sunlight, and it can be used for the location of real estate, and intervisibility studies.

• Determining rates of snow melt based on variations in sun shadow, which is influenced by slope, aspect, and elevation.

For ***the coal fire research***, the slope calculated from a DEM can be used to correct a satellite thermal image: the angle between the slope normal and the sun incidence line is calculated to simulate the solar heating image. This is subsequently subtracted from the day-time thermal image. The aspect helps to determine how much sun a site will receive. They are useful to separate false thermal anomalies from "real" thermal anomalies that are due to coal fires.
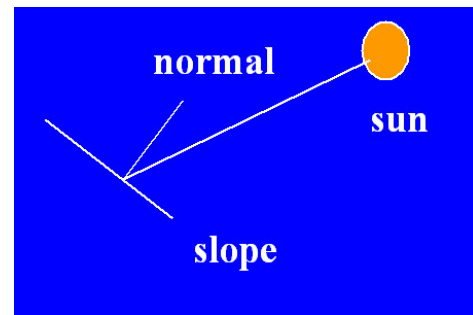
Moreover, the gradient of the surface on which a fire occurs is significant; steeper slopes promote fire spreading (Sofronov, 1964) and increase the rate of erosion (Menaut et al., 1995).

For the coal fire research project, a slope map and an aspect map were calculated from the DEM generated in this case study as shown in Figure 6.3 and Figure 6.4 respectively.
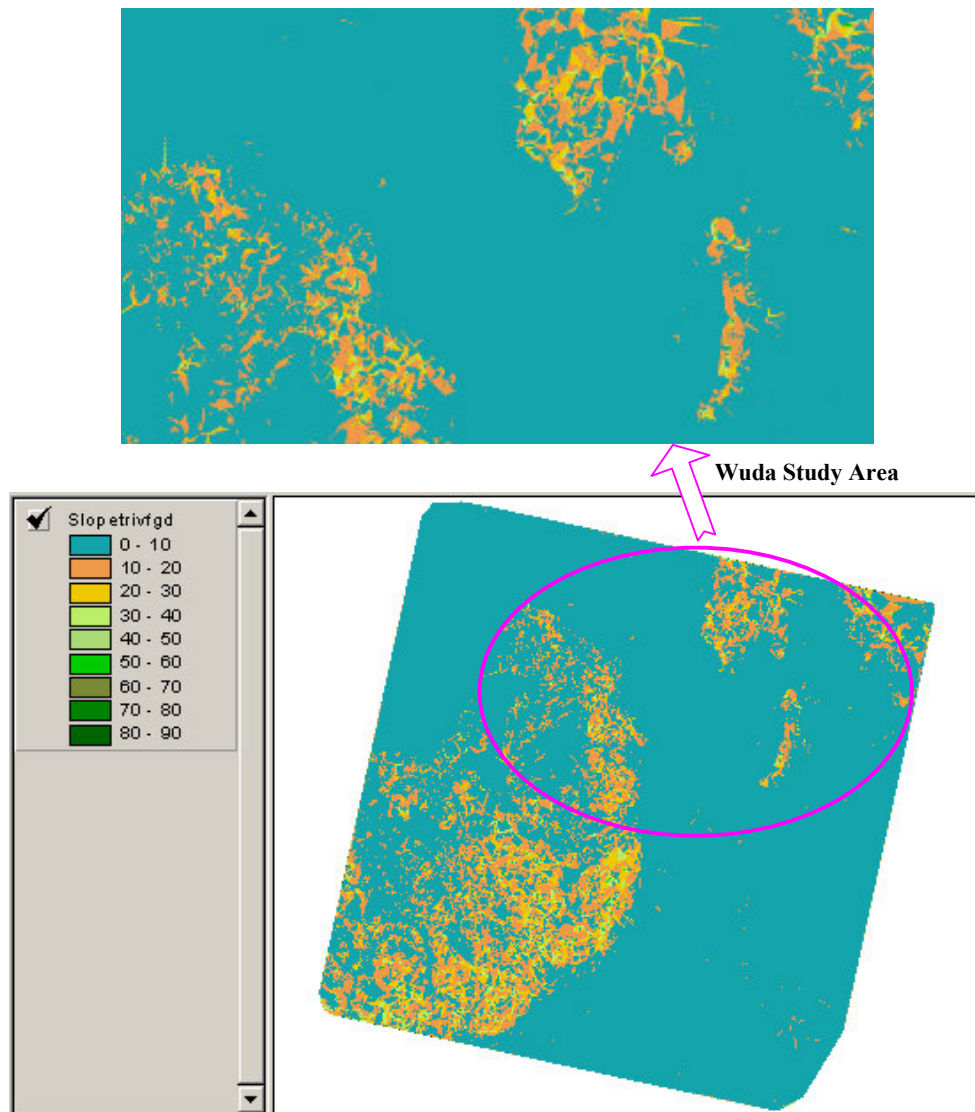
Fig 6.3: The slope element output for the Coal Fire Research Project

Wuda Study Area
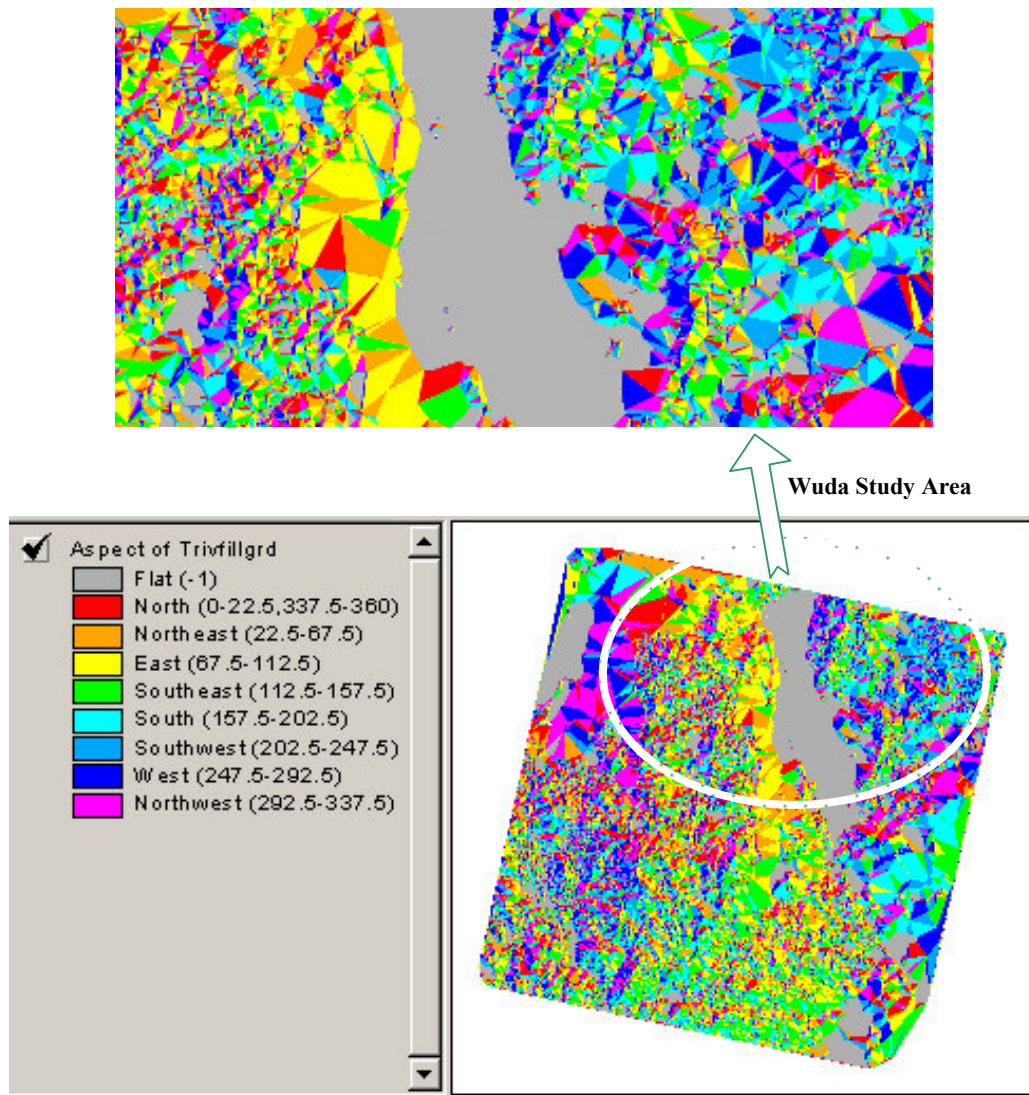
Fig 6.4: The slope aspect element output for the Coal Fire Research Project

7. Conclusion and Recommendation

7.1 Conclusion

The process to generate the DEM from an ASTER image pair was developed mainly in an empirical way. The result of the DEM evaluation shows a relatively acceptable accuracy of about 28m in height.

The key step in the extraction of a DEM is measuring Ground Control Points. Evenly-distributed, sufficient and accurate GCPs strongly influence the quality of the exterior orientation. A qualified exterior orientation leads to highly precisely estimated geometric model of the sensor when it captured the image. The well-restored sensor model in turn results in a highly accurate DEM.

In this case study, because the used mobile GPS in the field surveying had a large error in altitude coordinate, the z values of GCPs had to be collected by the aid of the topographic map.
Due to the use of a dated topographic map in a scale of 1:100,000 as the main ground data source, the photogrammetric task suffered from a lack of ideal GCP image measurement accuracy, GCP amount and distribution, may have contributed to a deterioration of the spot positioning accuracy.
Moreover, the ASTER image pair used for this DEM extraction has some low-correlation part, and these may have contributed in a deterioration of digital image matching computation, resulting in a relatively smaller number of mass points used in DEM interpolation.

However, the abovementioned situation may occur in most tasks of DEM extraction involving remote sensing data.
For example, usually it is difficult and uneconomical to obtain adequate ground control points over the entire image extent. Thus, extra data, mostly of different accuracy, is always needed for eliminating the distortion of the computed geometric model of the sensor as much as possible. This is to match the request of evenly distributed ground control points during DEM extraction.
Another actual status is that many low-to-medium resolution satellite remote sensing data, as data source, have relative low-correlation. Thus more control points are needed for efficiently restoring the geometric model of the sensor. Other than evenly-distributing the GCPs, including obtaining the data covering those low-correlating areas, adequate GCPs for the whole image scene are necessary.
As for the accuracy of the GCPs, it is the basis used to judge whether the photogrammetric results are reliable. In this case, a relatively small scale map was used for points measurement for exterior orientation, which can result in weak GCPs accuracies. The triangulation report and DEM extraction report are very important references to modify the preliminary results. Through the methodology adopted in this study, the final accuracy matches the precision of the input data source. The result of the DEM extraction using the ASTER image pair in this research is acceptable, and the methodology is efficient.

In general, DEM extraction from ASTER image pairs should consider the number, distribution, and accuracy requirements of GCPs, including all terrain types. All the aforementioned elements influence the ultimate accuracy of the DEM.

In conclusion, using the ASTER image pair to derive the DEM is worthwhile; the accuracy is acceptable on the basis of suitable data sources and proper operations.

7.2   Recommendation

The precision of the data source limits the final accuracy of the DEM extracted. Nevertheless, it would be possible to achieve higher accuracy by:

- acquiring data sources in sufficient accuracy such as latest medium-to-large scale topographic maps, high-resolution aerial photos. According GeoSystems (2002), a 50k topographic map (1:50,000) can meet the general accuracy requirement for DEM extraction. The larger scale the map is, the more details the information can give, and the higher precise the ground control points can be used as input. At the same time, the more the data (maps) a case can obtain, the higher the accuracy for sensor model, thus the higher the accuracy of the derived DEM.

- utilizing highly-precise surveying equipment e.g. Differential GPS receivers to measure GCPs at higher accuracy. By this way, the final DEM can be improved having a significantly higher accuracy.

- referencing good extra DEMs for acquiring supplementary data in some areas where GCPs were difficult to be measured.

- properly using data. If the conditions for acquiring data are optimal:
  1) GCPs is preferable to be measured from the sources of a same accuracy range in order to escape from large distortion.
  2) In mountainous area, the source data for GCPs input needs to be in higher because of the frequently changing terrain relief. While in plain area, the resolution of source data could be lower due to fewer changes in the terrain.

- the potential for using platform ephemeris and attitude data to supplement or replace GCPs. If ephemeris and attitude data of sufficient accuracy to calculate the transformation coefficients between the map and image coordinates system are available, the requirement for GCPs are greatly reduced. Although the accuracies of these DEMs, with widely spaced ground control, could be degraded compared to DEMs produced with full ground control, this approach which is using ephemeris and attitude data in conjunction with certain amount of GCPs, does result in DEMs that are sufficiently accurate in remote or unmapped areas within the extent of the original image pair. That is effective for creating ortho-image products or for the application of topographic correlations for other remote sensing data products.

- further editing.
  1) In Erdas Stereo Analyst the generated contour map from the DEM could be improved by editing the contour lines according to the terrain trends, to improve the output DEM; also stereoscopic interpretation and 3D-digitization according to the features could be performed. This will be optimal by the aid of high-quality ancillary topographic data to edit specific areas on the image extent.

2) Some parts have low-correlation or cloud and shadow cover, resulting in lack of mass points and unwanted deterioration of the ultimate DEM generating results. In this case a ground truth dataset is needed to further edit and evaluate the extracted DEM. Usually, these parts could appear as "holes" in a DEM image. From the point of image enhancement, some operations could be performed in the stage of data preprocessing for better extracting a DEM. Fortunately, the area of cloud cover in the image pair used for DEM extraction in this study is out of our interest for the coal fire research project, therefore this step was eliminated. For further study, for instance utilizing the whole image data, this technique of removing clouds on satellite images needs to be involved.

After extracting the DEM, some validation sites to assess the quality of the DEM are needed. The accuracy obtained determines the possibilities for employing the DEM for mapping, environmental assessment and geological studies, etc. All of these sites should be equipped with highly accurate topographic data, including the DEM, as well as GPS and photogrammetric survey data to evaluate the accuracy of the DEM result.

References

Altmaier, A., Kany, C., 2002, *Digital Surface Model Generation from CORONA Satellite Images*, ISPRS Journal of Photogrammetry & Remote Sensing 56 (2002), 221-235

ArcView 3D Analyst, Environmental Systems Research Institute, Inc., 2002

ASTER (Advanced Spaceborne Thermal Emission and Reflection Radiometer),
http://asterweb.jpl.nasa.gov, 2002

ASTER Digital Elevation Model, http://edcdaac.usgs.gov/aster/ast14dem.html, 2002

DEM-digital elevation model,
http://www.dfd.dlr.de/projects/coalfire/Remote_sensing_project/html/dem.html, 2002

Davis A.M., Liu J.G., Remote Sensing Unit, Earth Sciences, T.H. Huxley School, Royal School of Mines, Imperial College, London. *DEM Generation using ASTER stereo imagery,* 2001

DEM and Orthoimage from ASTER Data, Geosystems, 2002

Digital Elevation Models: the most accurate elevation datasets available,
http://www.spotimage.fr/home/proser/elevat/dem/welcome.html , 2002

"ERDAS IKONOS Sensor Model Support" Tour Guide, Erdas, 2001

Fujisada H., *ASTER Level-1 Data Processing Algorithm,* IEEE TRANSACTIONS ON GEOSCIENCE AND REMOTE SENSING, VOL.36, No.4, July,1998

IMAGINE OrthoBASE™ User's Guide, Erdas, 2001

Inner Mongolia, http://drlee.org/mongolia/innermon.html, 2002

Kiyingi K.G., *Integration of Digital Elevation Models and GIS,* ITC, May, 1998

Maathuis, B.H.P., van Genderen, J.L., DEM-extraction and Ortho-image generation from ASTER data, International Institute for Geo-information Science and Earth Observation (ITC), Presented at International Conference "Geographical Study of Central Asia and Mongolia", 6-11 September, 2002

Tokunaga, M., Hara, S., *DEM Accuracy Derived from Aster Data,*
http://www.gisdevelopment.net/aars/acrs/1996/ts10/ts10007.shtml , ACRS 1996

Olesonr, *ASTERDEM Production Flow,* 2002

Rosema, A. et.al, *Development and Implementation of a Coal Fire Monitoring and Fighting System in China,* "Manual of Coal Fire Detection and Monitoring", BRSC/EARS/ITC/NITG-TNO, 1999

Satellite Image, http://www.geosig.com/ptsatellite.htm, 2002

Service Stereo DEM Generation, http://dib.joanneum.ac.at/fe_serv/stereo_dem_gen.html, 2002

Specifications of the IKONOS satellite, http://www.met.ed.ac.uk/~alastm/spec.html, 2002

The SRTM global Mapping Mission... almost 2 years later!, Glenn Letham, Jan. 24, 2002, http://spatialnews.geocomm.com/features/srtm_jan2002/

Toutin, T., Dr. Cheng, P., *DEM Generation with ASTER Stereo Data,* June, 2001

Thomas M. Lillesand, Ralph W. Kiefer, *Remote Sensing And Image Interpretation*, John Wiley&Sons, Inc., Fourth edition, 2000

Welch R., T.J., H.L., and H.M., *ASTER as a source for Topographic Data in the Late 1990's*, IEEE Transactions on Geosciences and Remote Sensing, Vol.36, No.4, July 1998.

Wuhai of Inner Mongolia forms the largest coalfield fire zone of China, Science Times (2002-01-18), http://www.enviroinfo.org.cn/Disasters/Fire/e012142_en.htm, 2002

Yamaguchi Y., A.B.K., H.T., T. K., and M.P., *Overview of Advanced Spaceborne Thermal Emission and Reflection Radiometer (ASTER),* IEEE TRANSACTIONS ON GEOSCIENCE AND REMOTE SENSING, VOL.36, No.4, July,1998.

Appendices

Appendix A: DEM FILL Avenue Script

```
Name: Spatial.DEMFill
' ' Title: Creates a grid theme by filling all sinks in another grid theme.
'' Topics: Spatial Analyst, Hydrological modeling
'' Description: Takes a grid theme and fills all sinks, areas of
' internal drainage, contained within it. The aGrid.FlowDirection,
' aGrid.Sink, aGrid.Watershed, aGrid.ZonalFill, and aGrid.Con
' requests is used to fill the sinks. The process of filling
' sinks can create sinks, so a looping process is used until all
' sinks are filled. One cell sinks are not filled. Sinks of
' any depth are filled.
' Requires: The Spatial Analyst extension to be loaded. The script
' also requires an active view with an active grid theme that
' represents a surface. The grid theme should be the only active
' theme in the view.
'
' Self:
'
' Returns:
'
theView = av.GetActiveDoc

' fill active GTheme
theTheme = theView.GetActiveThemes.Get(0)

' fill sinks in Grid until they are gone
elevGrid = theTheme.GetGrid
sinkCount = 0
numSinks = 0
while (TRUE)
  flowDirGrid = elevGrid.FlowDirection(FALSE)
  sinkGrid = flowDirGrid.Sink
  if (sinkGrid.GetVTab = NIL) then
    ' check for errors
    if (sinkGrid.HasError) then return NIL end
    sinkGrid.BuildVAT
  end
  ' check for errors
  if (sinkGrid.HasError) then return NIL end
  if (sinkGrid.GetVTab <> NIL) then
    theVTab = sinkGrid.GetVTab
    numClass = theVTab.GetNumRecords
    newSinkCount = theVTab.ReturnValue(theVTab.FindField("Count"),0)
  else
    numClass = 0
    newSinkCount = 0
  end
  if (numClass < 1) then
    break
  elseif ((numSinks = numClass) and (sinkCount = newSinkCount)) then
    break
  end
  waterGrid = flowDirGrid.Watershed(sinkGrid)
  zonalFillGrid = waterGrid.ZonalFill(elevGrid)
  fillGrid = (elevGrid <
(zonalFillGrid.IsNull.Con(0.AsGrid,zonalFillGrid))).Con(zonalFillGrid,elevGrid)
  elevGrid = fillGrid
  numSinks = numClass
  sinkCount = newSinkCount
end
' rename data set
aFN = av.GetProject.GetWorkDir.MakeTmp("fill", "")
elevGrid.Rename(aFN)
' create a theme
theGTheme = GTheme.Make(elevGrid)

' set name of theme
theGTheme.SetName("Filled"++theTheme.GetName)

' add theme to the view
theView.AddTheme(theGTheme)
```

Appendix B: Additional References without Being Cited

ASTER Data Products, http://edcdaac.usgs.gov/aster/asterdataprod.html, 2002

Bohnenstiehl K. R., Denver, *Monitoring Surface Coal Mining* [www.wrcc.osmre.gov], 2002

Childs, J., technical editor Paul Burkhardt, *ASTER DEM!* ,http://www.terrainmap.com/, 2002

Childs, J., *Terrain Modeling and Mapping using DEM, SDTS, DRG, DLG, DTED ASTER, Landsat, EarthSat and EarthKam Data,* http://www.terrainmap.com/rm103.html#aster, 2002

Glasspool, I., *A major fire event recorded in the mesofossils and petrology of the Late Permian, Lower Whybrow coal seam, Sydney Basin, Australia,* Palaeogeography, Palaeoclimatology, Palaeoecology 164 (2000) 373-396

ITC's investigations in China's coalfields, http://www.itc.nl/personal/coalfire/activities/dlr.html#testarea, 2002

Jensen, J. R., *Introductory Digital Image Processing, A remote sensing perspective,* Prentice-Hall, A Division of Simon & Schuster, Inc., 1986

Lodwick, *G. D., Digital Terrain Modelling,* The University of Calgary, August, 1983

Sharif, M., *DEM Optimization Using Satellite Images*, ITC, 1996

Technology Support: Products of Erdas Imagine, www.superfull.com, 2002

Wolf, P.R., Dewitt, B.A., *Elements of Photogrammetry with Applications in GIS,* The McGraw-Hill Companies, Inc., 2000, 1983, 1974

Appendix C: Triangulation Report

```
              Triangulation Report With OrthoBASE
              Output image units: pixels
              Output ground units: meters
              Output angular units: radians

Points excluded with gross errors:
  image     pid      image_x       image_y      residual_x   residual_y
     1       29     733.9453     2058.6328       -2.3347      -3.3098
     1       22    1163.2812      776.0312       -0.1822      -2.0765
     1       36    1904.7891      878.8516       -0.6637       1.7811
     1       75    3645.9766     1525.0078       -2.0118       0.4933
     1       70    2478.2734     1878.2578       -0.8178      -2.1423
     1       59    1615.8789     1571.1914       -1.6595       1.6565
     1       61    3889.2227     1046.7383       -1.8267      -1.7882
     1       11    3666.9766     1945.1797       -1.4847       1.6878
     1       63    3398.5078     3594.9453        2.2993      -0.8867
     1        4     379.0547     3105.3828        1.7970       1.7004
     1        1     817.7227      355.7852        2.0241      -1.4774
     1       79    3423.5078     3421.5078       -2.4683       1.0376
     1       82    2598.7891     2483.2266       -0.0133      -2.0692
     1       18    1260.6685      581.5801        1.9157      -1.4784
     1       87     607.9766     3191.0391        2.2880       0.4847
     2        3    1572.7187     2113.2188       -0.4591       1.9976
     2       29    1250.9609     2467.6016        0.1191      -2.5259
     2       95    3965.9883     2172.9883        2.4248       0.9822
     2       93    4116.0078     1843.0078        2.2464      -0.1237
     2       22    1721.2812     1232.0938        0.6769      -2.1728
     2       78    3704.8047     3810.7891       -1.9922      -0.2250
     2       70    3167.2734     2289.2734        0.9102       2.0057
     2       53    1248.7695     2298.8477        0.9916       1.9686
     2       54    1410.8745     2215.1253        2.2229      -0.5800
     2       59    2225.9453     1999.0703       -2.6668       1.3568
     2        9    4284.6641     2368.2891        2.1059       0.3490
     2       14    4247.3516     2631.3203        1.9932       0.2807
     2       63    4172.5078     3945.9453       -2.7293       0.9731
     2        4     869.0859     3479.3516       -2.4363      -1.7476
     2        1    1324.7852      818.7852       -2.0673       1.6344
     2       51     959.1869     2501.0627        1.9587       0.4149
     2       79    4187.5938     3782.4688        2.9462      -1.1891
     2       82    3271.7578     2869.1953        0.2372       2.1473
     2       18    1833.5154     1041.6723       -1.9896       1.5781
     2       87    1120.0078     3559.0078       -2.7851      -0.4551

Normal weighted iterative adjustment:
  No.  Total_RMSE Max_Residual at image pid
   1    0.448344   -1.8941         2    74
   2    0.447337   -1.8964         2    74

Image parameter value and precision:
 image id 1:
      x:  5.19089248e+005 -1.74786350e+003 -5.68419254e+000
          4.22038772e+002  8.43152205e+001  2.17535505e-001
      y:  4.34330628e+006  3.88193591e+003 -1.60910628e-001
          4.46167191e+002  7.81250727e+001  5.84516964e-002
      z:  8.62692271e+005 -2.59873213e+002  4.20394555e+001
          1.41125778e+002  2.60339639e+001  1.36259210e+000
  omega:  9.93714854e-003 -1.64995563e-003
          5.17917565e-004  9.02377941e-005
    phi: -1.41727762e-001 -2.63055068e-003
          5.00107681e-004  9.97352980e-005
  kappa: -1.83141277e-001  1.13699914e-004 -5.94189343e-006
          8.79186406e-005  7.88998140e-006  1.21013940e-006
 image id 2:
      x:  4.80354288e+005 -7.76895315e+003  1.48542686e+001
          4.09280426e+002  7.25625163e+001  3.38510596e-001
      y:  3.90224548e+006  3.33706147e+003  9.08232617e+000
          3.93424969e+002  1.34004833e+002  4.91569144e-001
      z:  7.58600453e+005 -2.52961754e+003 -1.17959041e+001
          2.74901706e+002  7.99967415e+001  4.97441614e-001
  omega:  5.36574185e-001  4.35120901e-004
          5.06494888e-004  1.74105251e-004
    phi: -1.80538816e-001 -8.98831849e-003
          4.81661076e-004  8.56676581e-005
  kappa:  1.56602457e-002  2.01748285e-004 -2.49917830e-005
          9.60167900e-005  8.92078289e-006  1.28246708e-006
```

```
Ground point value and precision in parenthesis:
 point id      3:    648183.0595 ( 0.0030)   4370941.0041 ( 0.0030)   1120.0000 ( 0.0030)
 point id      5:    640516.1850 ( 5.8866)   4368688.8770 ( 6.2087)   1200.0000 ( 0.0030)
 point id     10:    647343.3849 ( 0.0030)   4373354.3344 ( 0.0030)   1126.0000 ( 0.0030)
 point id     12:    646494.9026 ( 0.0030)   4373028.4467 ( 0.0030)   1132.0000 ( 0.0030)
  point id    13:    662277.1999 ( 5.9431)   4371894.0199 ( 6.2036)   1179.0000 ( 0.0030)
```

·· (similar sigma omitted)

```
point id    218:    650307.2752 ( 6.1968)   4333990.6118 ( 7.5645)   1209.6422 (19.8064)
 point id   219:    650057.7230 ( 6.2519)   4338949.4944 ( 7.5202)   1185.8184 (19.6470)
 point id   220:    648257.7299 ( 6.7729)   4369689.8135 ( 7.3560)   1155.0893 (18.6588)
 point id   221:    648562.4886 ( 6.4936)   4353691.6752 ( 7.4819)   1222.0854 (19.3094)
 point id   222:    648767.6666 ( 6.1404)   4328965.2023 ( 7.6390)   1219.9273 (20.0339)
```

·· (similar sigma omitted)

```
Control and check point residuals in meters:
 type     pid     residual_x        residual_y        residual_z
 gcp        3      0.00000667       -0.00000228        0.00000086
 gcp        5                                          4.80486655
 gcp       10      0.01227945        1.00100448        0.75113521
 gcp       12     -0.04190887        0.86219117        0.91523735
 gcp       13                                         -7.39062482
 gcp       15                                         -6.26588444
 gcp       19                                         -4.40757265
 gcp       20      0.82159387        0.11139753       -3.59009240
 gcp       21                                         -0.73038536
 gcp       28                                          1.64524278
 gcp       30                                         -2.22338859
 gcp       31                                          4.86277588
 gcp       35                                          5.96847505
 gcp       38     -0.52091572       -0.43879717        2.43066996
 gcp       37                                          5.14838405
 gcp       39                                          1.81280583
 gcp       17                                         -6.08034729
 gcp       24                                         -2.22618589
 gcp       25                                          0.32400188
 gcp       26      0.14836855        1.38286554        0.38122455
 gcp       27      0.13326841        1.36400643        0.43763114
```

·· (similar sigma omitted)

```
gcp      102      0.90332630        0.11187607       -3.94553193
 chk      313      2.77416845        0.91897740       -8.64292109
 chk      314    -10.51181592       -1.30289003        1.86702483
 chk      315                                         -4.72913150
 chk      316    -13.21080178      -27.69827167       -5.06178378
 chk      317    -13.04935667        0.93170825      -10.11821524
 chk      318     12.08757133        1.59149381       15.05213358
 chk      319                                          4.29221163
 chk      321      1.45992306      -12.64908913       -8.67549781
Image points and their residuals:
 image    pid       image_x        image_y       residual_x       residual_y
    1       3     1023.3382      1691.9978        -0.3727           0.8025
    1     102      891.5792       667.6731        -0.1794           1.1974
    1      10      885.1288      1733.5472        -1.7228          -0.3669
    1      12      902.7979      1778.7584        -1.1161          -2.0619
    1     101     1179.4467       637.4514        -0.1989           0.8022
    1     100     2875.4009      1369.7721        -0.3881          -0.3920
    1      99     2110.3532      1466.9864         0.1266           0.1974
    1      20      737.7020       916.5629        -1.1728          -1.3123
```

·· (similar sigma omitted)

```
    2       5     1700.8256      2508.4863         0.8725           0.4394
    2     102     1420.1060      1127.0488        -0.8527           0.5797
    2      10     1419.9168      2155.1423        -0.9035           0.1970
    2      12     1439.1201      2198.5965         0.2061          -1.1925
    2     101     1737.2890      1098.1517        -2.1715           0.4161
    2     100     3611.9396      1805.0032         2.1505          -0.2233
    2      99     2766.6928      1897.8501        -0.4712           0.0297
    2      20     1255.0595      1367.7897         2.1455          -0.0619
    2      98     2592.5585      1940.0329         0.3944          -0.7249
    2      97     1111.9742      3236.8727        -1.7641          -0.9281
    2     321     2391.7567      1682.6790        -0.3370           0.6478
    2      96     3351.6661      1330.6785        -0.3378           1.1746


Image accuracy for control and check points for each scene:
 image id 1:
      pid   type     image_x        image_y       residual_x       residual_y
        3   gcp     1023.7109      1691.1953        -0.3727           0.8025
      102   gcp      891.7587       666.4758        -0.1794           1.1974
       10   gcp      886.8516      1733.9141        -1.7228          -0.3669
       12   gcp      903.9141      1780.8203        -1.1161          -2.0619
      101   gcp     1179.6456       636.6492        -0.1989           0.8022
```

```
  100   gcp    2875.7891    1370.1641     -0.3881     -0.3920
   99   gcp    2110.2266    1466.7891      0.1266      0.1974
   20   gcp     738.8748     917.8752     -1.1728     -1.3123
   98   gcp    1952.1953    1510.7891      0.3902      0.1259
   97   gcp     610.8008    2857.8164      0.5166      1.7448
   96   gcp    2641.9414     877.5352     -0.4257     -0.5120
   95   gcp    3200.9883    1752.9883     -0.7979      0.6340
   94   gcp    3584.9453    1727.7578     -1.7570      0.9693
   38   gcp    1283.7852    1713.7539      1.8134      0.7642
   93   gcp    3337.0195    1409.0039     -0.4886      0.1456
   89   gcp     583.8789    1488.9102      0.0115     -0.6377
   88   gcp     365.0078    2432.0078      1.7200      0.7708
   86   gcp    2292.2891    1454.7578     -0.1008     -0.5426
  321   chk    1769.0313    1244.0313      0.2570     -0.6747
   85   gcp    2450.0195     596.4414      1.0080     -0.2334
   84   gcp    2917.7578    1055.2266      0.1172     -0.6053
   26   gcp     822.3203    1630.3203      0.2682     -0.9709
   27   gcp     870.1246    1589.8752      1.2356     -0.2002
   32   gcp    1399.2383    1665.8164      0.4898     -0.8640
   33   gcp    1582.7539    1136.8164     -0.9879      1.1334
   83   gcp    2839.1953     609.1641     -0.8091     -0.9423
   81   gcp    2422.9766    3324.9453      0.5194     -0.6308
   80   gcp    2415.2578    3597.7266      1.6032      1.3964
   78   gcp    2971.7734    3453.7578      0.0630     -0.1437
   77   gcp    3357.9766    1115.0078     -1.1519     -1.3544
   76   gcp    3407.7266    1762.7891     -0.8162      0.7998
  318   chk     650.7188    1692.3438      0.1921     -0.3047
   73   gcp    2474.7578     965.0078      0.5394     -0.4031
   72   gcp    1878.9766    3149.9766      1.3597     -0.2271
   71   gcp    2222.0078    3197.3203      0.8453     -0.8503
  317   chk    1316.0313    2588.0313      0.2785     -1.1959
   50   gcp     746.2266    2656.3516     -1.7205      1.4018
   69   gcp    2179.7578    1939.1953      0.0024      0.0410
   52   gcp     597.1953    1915.1953      0.8787     -1.3616
   53   gcp     730.7891    1883.8203     -0.6017      0.9327
   54   gcp     877.8203    1796.1328      1.6183     -0.6224
   68   gcp    1714.0078    1628.9766     -0.0140     -0.2540
   67   gcp    1957.6641    1719.3359      0.6299     -0.3303
   57   gcp    1360.6914    2442.1914     -1.8221     -0.2947
   66   gcp    1893.0078    2284.0078     -0.0648      0.2422
  316   chk    1819.0938    1368.9688      0.0706      0.6339
   65   gcp    3125.9922    2482.9453     -1.4050      0.2089
   62   gcp     888.7891     148.8203      0.2438      0.8962
   64   gcp    2876.1328    2843.0078      0.1606     -1.5406
    2   gcp     370.7266    2997.7266      0.8118      1.0548
   16   gcp    3501.9766    3058.0234     -0.6706     -0.9266
    6   gcp    3244.7266    3798.2266     -0.2706     -1.1703
    7   gcp    3332.7578    3768.1641      1.0568     -0.3592
    8   gcp    3026.7266    1446.8203     -0.6179     -0.6068
    9   gcp    3489.7109    1955.2734     -0.6191      0.6678
  314   chk    1262.9688    1614.0313      0.0488     -0.0218
   14   gcp    3456.3047    2228.2891     -1.3436      1.0663
  313   chk    1051.5309    1641.9690      0.0652     -0.1170
  RMS Errors for    52 GCPs:   x:       0.9440
                               y:       0.8741
                           total:       1.2865
  RMS Errors for     6 CHKs:   x:       0.1789
                               y:       0.6317
                           total:       0.6565
image id 2:
  pid   type    image_x      image_y      residual_x  residual_y
  102   gcp    1420.9587    1126.4691     -0.8527      0.5797
   10   gcp    1420.8203    2154.9453     -0.9035      0.1970
   12   gcp    1438.9141    2199.7891      0.2061     -1.1925
  101   gcp    1739.4606    1097.7356     -2.1715      0.4161
  100   gcp    3609.7891    1805.2266      2.1505     -0.2233
   99   gcp    2767.1641    1897.8203     -0.4712      0.0297
   20   gcp    1252.9141    1367.8516      2.1455     -0.0619
   98   gcp    2592.1641    1940.7578      0.3944     -0.7249
   97   gcp    1113.7383    3237.8008     -1.7641     -0.9281
  321   chk    2392.0938    1682.0313     -0.3370      0.6478
   96   gcp    3352.0039    1329.5039     -0.3378      1.1746
   94   gcp    4388.9766    2148.7266      1.9204      1.6272
   38   gcp    1857.7695    2134.7852      1.7900      1.6011
  318   chk    1163.5938    2115.4063     -0.3163      0.0999
   89   gcp    1089.8633    1919.9258     -1.0783     -0.7751
   88   gcp     849.0078    2828.0078     -2.2357     -0.9088
   86   gcp    2966.2109    1885.7734      1.0546     -0.1098
  317   chk    1880.0313    2972.0938     -0.2693      1.0677
   85   gcp    3141.0039    1060.4492     -1.5207     -0.4678
   84   gcp    3657.7578    1502.2266      0.5999     -0.2643
   26   gcp    1351.3398    2055.3242      0.5852     -0.2666
```

```
 27  gcp    1404.1016    2015.8828     1.6085     0.9883
 32  gcp    1985.2070    2089.8320     0.3152    -1.1509
 33  gcp    2184.7383    1580.8008    -0.5080     0.2447
 83  gcp    3568.2266    1072.1328     0.3723     0.2680
 36  gcp    2538.8164    1331.8633    -0.6745     1.3889
 81  gcp    3097.0078    3685.0703     1.5004    -0.1174
 80  gcp    3092.2578    3949.7578    -1.3785     0.2557
316  chk    2448.0313    1805.0313    -0.3452    -0.6970
 77  gcp    4140.9766    1559.9766     0.8382    -0.8718
 76  gcp    4194.7578    2182.7891     2.4210     1.0932
 75  gcp    4456.9766    1954.9766     0.2688     0.0079
 73  gcp    3167.7891    1414.0078     0.7111     0.7031
 72  gcp    2502.0078    3517.0078    -0.4719    -1.0377
 71  gcp    2877.0234    3562.3047    -2.0210    -1.2393
 50  gcp    1261.2539    3042.3008     0.0680     1.2768
 69  gcp    2837.7578    2351.1953     0.0117     0.4505
 52  gcp    1104.2070    2329.1758     1.6882    -0.0048
314  chk    1835.9688    2039.9688    -0.3452    -0.1311
313  chk    1603.6563    2066.9063    -0.3614    -0.0683
 68  gcp    2330.0078    2053.9766    -0.7210    -0.6475
 67  gcp    2596.6797    2140.3047     0.5244    -0.2567
 57  gcp    1932.7266    2834.1953    -1.1925     0.4840
 66  gcp    2517.0078    2682.0078    -1.1980     0.6274
 65  gcp    3877.9922    2874.9766    -2.2318     0.8757
 61  gcp    4725.2227    1494.7539    -1.2544    -1.6250
 62  gcp    1413.8164     627.8789    -1.6239    -1.4793
 64  gcp    3587.1953    3218.0234     0.5996     1.8877
  2  gcp     854.7383    3372.7539    -0.6179    -0.6446
 16  gcp    4296.0078    3430.0547     0.3340    -1.4635
  6  gcp    4000.7578    4142.1953    -1.7667     0.3452
  7  gcp    4101.7578    4114.2266     0.2317     0.1082
  8  gcp    3776.6953    1879.7891     0.7951    -1.1890
 11  gcp    4478.9922    2358.1641     2.4545     1.8075
RMS Errors for    48 GCPs:   x:      1.3057
                             y:      0.9217
                         total:      1.5983
RMS Errors for     6 CHKs:   x:      0.3304
                             y:      0.5884
                         total:      0.6748


Summary RMSE for GCPs and CHKs (number of observations in parenthesis):
            Control                    Check
 Ground X:    0.6127  (56)          10.0933 (6)
 Ground Y:    1.1758  (56)          12.4709 (6)
 Ground Z:    3.4491  (89)           8.2825 (8)
 Image  X:    0.7518  (165)          0.5710 (16)
 Image  Y:    1.0592  (165)          0.2502 (16)
```

Appendix D: DEM Extraction Report

```
                       Date Created: 02/17/03
                       Time Created: 18:37:57


DTM PROJECT INFORMATION

    Block File Used: shiftvert.blk
    Block File Location: k:/xo/wuda/achievement/final/result/
    DTM Correlation Time (seconds): 107
    Points Per Second: 295
    Total Processing Time (seconds): 107

    DTM Type: 3D Point Shapefile
    DTM Name: k:/xo/wuda/achievement/final/result/finalshp.shp
    Number of Mass Points Extracted: 31620
    Upper left corner of DTM Bounding Box: (607598.2507, 4386716.3088)
    Lower right corner of DTM Bounding Box: (678094.2051, 4317338.7401)

    Minimum Mass Point Elevation: 1002.3854
    Maximum Mass Point Elevation: 2484.6194
    Mean Mass Point Elevation: 1421.2095

    Projection: UTM
    Spheroid: WGS 84
    Datum: WGS 84
    Horizontal Units: meters
    Vertical Units: meters

    Strategy Parameter Settings:

        Image Pair Name: b3nrot_b3brot
            Region Description: Default Region
            Name of Strategy Used: Low Urban
            List All of the Strategy Parameter Values Used:
                Search Size: 11 x 3
                    Allow Adaptive Change: Yes
                Correlation Size: 7 x 7
                    Allow Adaptive Change: Yes
                Coefficient Limit: 0.8000
                    Allow Adaptive Change: Yes
                Topographic Type: Rolling Hills
                Object Type: Low Urban
                Use Image Band: 1
                DTM Filtering: high

            Region Description: no description
            Name of Strategy Used: Exclude Area
            Elevation of Exclude Area: undefined

            Region Description: no description
            Name of Strategy Used: Exclude Area
            Elevation of Exclude Area: undefined
```

.... (similar description omitted)

```
            Region Description: no description
            Name of Strategy Used: High Mountains
            List All of the Strategy Parameter Values Used:
                Search Size: 5 x 3
                    Allow Adaptive Change: Yes
                Correlation Size: 5 x 5
                    Allow Adaptive Change: Yes
                Coefficient Limit: 0.8000
                    Allow Adaptive Change: Yes
                Topographic Type: Mountains
                Object Type: Open Area
                Use Image Band: 1
                DTM Filtering: low

            Region Description: no description
            Name of Strategy Used: High Mountains
            List All of the Strategy Parameter Values Used:
                Search Size: 5 x 3
                    Allow Adaptive Change: Yes
                Correlation Size: 5 x 5
                    Allow Adaptive Change: Yes
```

```
                    Coefficient Limit: 0.8000
                        Allow Adaptive Change: Yes
                    Topographic Type: Mountains
                    Object Type: Open Area
                    Use Image Band: 1
                    DTM Filtering: low
```

.... (similar description omitted)

```
                Region Description: no description
                Name of Strategy Used: Low Urban
                List All of the Strategy Parameter Values Used:
                    Search Size: 11 x 3
                        Allow Adaptive Change: Yes
                    Correlation Size: 7 x 7
                        Allow Adaptive Change: Yes
                    Coefficient Limit: 0.8000
                        Allow Adaptive Change: Yes
                    Topographic Type: Rolling Hills
                    Object Type: Low Urban
                    Use Image Band: 1
                    DTM Filtering: high
```

.... (similar description omitted)

```
ACCURACY INFORMATION

    General Mass Point Quality:
        Excellent % (1-0.85): 52.6439 %
        Good % (0.85-0.70): 26.5117 %
        Fair % (0.70-0.5): 0.0000 %
        Isolated %: 0.0000 %
        Suspicious %: 20.8444 %

    Global Accuracy:

        Vertical Accuracy:
            Total # of 3D Reference Points Used: 46
            Minimum, Maximum Error: -50.3625, 61.2698
            Mean Error: 7.8272
            Mean Absolute Error: 23.4312
            Root Mean Square Error (RMSE): 28.1646
            Absolute Linear Error 90 (LE90): 48.9091
            NIMA Absolute Linear Error 90: +/- 25.7229


    User Defined Check Points to DTM Vertical Accuracy
        Total # of User Defined Check Points Used: 46
        Minimum, Maximum Error: -50.3625, 61.2698
        Mean Error: 7.8272
        Mean Absolute Error: 23.4312
        Root Mean Square Error: 28.1646
        Absolute Linear Error 90: 48.9091
        NIMA Absolute Linear Error 90: +/- 25.7229

        Detailed Point Accuracy Information:

            Pt.ID       X            Y               Z         DTM Z        Residual
             313    648183.0595   4370941.0041   1120.0000   1150.6379      30.6379
             314    647343.3849   4373354.3344   1126.0000   1142.6285      16.6285
             315    646494.9026   4373028.4467   1132.0000   1169.9118      37.9118
             316    662396.2641   4365432.5859   1210.0000   1185.2775     -24.7225
             317    661171.5780   4368818.6140   1170.0000   1173.2216       3.2216
             318    664588.0159   4356871.3421   1189.0000   1177.1506     -11.8494
             319    636975.9335   4366614.5663   1320.0000   1350.1483      30.1483
             320    648127.0641   4365459.3048   1126.0000   1138.4129      12.4129
             321    646968.6650   4366333.9881   1138.0000   1160.8318      22.8318
             322    646002.6174   4366287.5854   1149.0000   1172.0834      23.0834
             323    670280.3673   4366010.8398   1250.0000   1217.1519     -32.8481
             324    669342.2702   4367215.3154   1240.0000   1258.6892      18.6892
             325    665625.3893   4368794.8430   1208.0000   1225.6857      17.6857
             326    649195.3983   4375780.0926   1104.0000   1117.0293      13.0293
             327    649295.7750   4374487.6014   1108.0000   1116.9643       8.9643
             328    650064.9873   4373644.9909   1099.0000   1098.4181      -0.5819
             329    648861.1965   4364332.2372   1118.0000   1107.5853     -10.4147
             330    658872.7062   4361314.1064   1159.0000   1150.1516      -8.8484
             331    663367.2254   4356849.3931   1178.0000   1164.3266     -13.6734
             332    663872.6421   4355727.0413   1190.0000   1186.2252      -3.7748
             333    667376.6352   4356597.0604   1202.0000   1187.3608     -14.6392
```

334	662212.8275	4360569.1203	1218.0000	1219.1698	1.1698
335	659828.8627	4368656.3795	1170.0000	1231.2698	61.2698
336	640521.7049	4371961.6632	1260.0000	1311.2857	51.2857
337	643832.7527	4378329.9931	1120.0000	1168.9091	48.9091
338	644425.8096	4376022.3561	1139.0000	1178.3208	39.3208
339	646169.7490	4373432.8704	1130.0000	1176.6245	46.6245
340	632806.3360	4363299.3507	1438.0000	1473.8761	35.8761
341	634232.2783	4364766.0201	1400.0000	1453.2402	53.2402
342	650702.8170	4360591.1349	1105.0000	1132.0950	27.0950
345	623967.5374	4327072.5061	1320.9910	1351.9690	30.9780
346	627656.5566	4337976.7794	1881.9150	1919.9514	38.0364
347	634513.7561	4333764.4418	1464.2900	1434.1445	−30.1455
348	637483.9108	4355422.0645	1501.5190	1498.2132	−3.3058
349	648130.9717	4354481.6523	1220.0790	1204.2990	−15.7800
350	649694.0259	4358814.3494	1177.2430	1148.5852	−28.6578
351	644125.4254	4350503.0755	1332.0220	1344.8552	12.8332
352	620710.0996	4349288.2787	1684.6290	1634.2665	−50.3625
353	618465.7742	4345733.0046	1624.6020	1637.0881	12.4861
354	653299.7210	4348699.6416	1150.7030	1170.7117	20.0087
355	651900.8286	4378718.9594	1152.7210	1141.1262	−11.5948
356	655767.5036	4374869.5508	1660.7540	1632.6253	−28.1287
358	652038.0209	4354656.3673	1167.6130	1164.3975	−3.2155
359	652953.8088	4351894.9325	1154.2590	1158.8253	4.5663
360	668211.4692	4368551.4853	1292.2850	1249.1430	−43.1420
361	667584.1368	4373591.2504	1320.4470	1297.2399	−23.2071